Title

Simulating terrestrial carbon fluxes using the new biosphere model BEAMS: Biosphere model integrating Eco-physiological And Mechanistic approaches using Satellite data

Full names of authors

Takahiro Sasai[1], Kazuhito Ichii[2], Yasushi Yamaguchi[1], Ramakrishna Nemani[3]

[1] Department of Earth and Environmental Sciences, Nagoya University, Furo-cho, Chikusa, Nagoya, 4648602, Japan
(T. Sasai) Tel: +81-52-789-3023, E-mail: sasai@system.eps.nagoya-u.ac.jp
(Y. Yamaguchi) Tel: +81-52-789-3017, E-mail: yasushi@nagoya-u.jp

[2] San Jose State University, Moffett Field, CA, 94035, USA.
Tel: +1-650-604-6444, E-mail: kichii@arc.nasa.gov

[3] NASA Ames Research Center, Moffett Field, CA, 94035, USA.
Tel: +1-650-604-6185, E-mail: ramakrishna.r.nemani@nasa.gov

Corresponding Author

Takahiro Sasai

Running title

Plant Stress and Biosphere model

Abstract

In this study we present a new biosphere model called the Biosphere model integrating Eco-physiological And Mechanistic approaches using Satellite data (BEAMS). BEAMS provides a new method of calculating the environmental stress affecting plant growth (Stress). Stress is calculated eco-physiologically using a photosynthesis model and stomatal conductance formulation, providing a more realistic result than previous models. Stress values are used to estimate Gross Primary Production (GPP) estimates via the light use efficiency concept. We used BEAMS, including our new Stress approach, to investigate global spatial and temporal patterns of Net Primary Production (NPP) and Net Ecosystem Production (NEP). BEAMS was run for the years 1982-2000 using global-scale satellite and climate data. Comparison of model results with observational measurements at flux sites reveals that GPP values predicted by BEAMS agree with measured GPP. Obtained Stress values were compared with those of MOD17 and CASA; the three methods produce contrasting spatial patterns. Upon comparing predicted and observed NPP, the pattern of NPP for each plant functional type can be adequately estimated. In terms of trend analysis, NPP increased for the years 1982-2000 in most regions. Different NPP trends were observed in Europe, Russia, and northeast Canada than those proposed by Nemani et al. [2003]; we attribute these differences to climate-related processes. Simulated inter-annual variations in global NEP are similar to results from inverse modeling. A sensitivity study of obtained NEP shows that the inter-annual variability in NEP is strongly controlled by air temperature, precipitation, CO_2, and the fraction of absorbed photosynthetically active radiation.

1. Introduction

Atmospheric CO_2 concentration is strongly controlled by the terrestrial biosphere. Net Primary Production (NPP) and Net Ecosystem Production (NEP) represent the rates of atmospheric carbon uptake by vegetation and the carbon exchange between the atmosphere and biosphere, respectively, both of which play important roles in the terrestrial carbon cycle. Accurate estimates of the spatial and temporal patterns of NPP and NEP are necessary to understand both the current-day and future terrestrial carbon cycles, which have a strong affect on global environmental change. Importantly, quantitative estimates of regional- and global-scale NPP and NEP values are extremely difficult to obtain, as these fluxes cannot be directly measured at a large scale.

A number of biosphere models have previously been proposed as a means of estimating the spatial pattern of NPP and NEP fluxes. These models are of two types: diagnostic models that require satellite and climate data as input parameters [e.g., Potter et al., 1993; Ruimy et al., 1996], and prognostic models that require only climate data as input parameters [e.g., Warnant et al., 1994; Foley et al., 1996; Kucharik et al., 2000; Sitch et al., 2003]. Existing global biosphere models produce contrasting estimates of annual global NPP, ranging from 40 to 80 GtC/yr [Cramer et al., 1999, Ruimy et al., 1999]. This uncertainty indicates the need to develop a more realistic and accurate method of calculating global carbon fluxes.

Accurate calculation of Gross Primary Production (GPP) is required for estimating NPP and NEP. One of the primary methods of calculating GPP is the Light Use Efficiency (LUE) concept, which assumes that photosynthesis productivity is proportional to light absorption [Monteith, 1972, 1977; Asrar et al., 1984]:

$$GPP = APAR * LUE = (FPAR * PAR) * (LUEmax * \mathit{Stress}) \quad (1)$$

where PAR is Photosynthetically Active Radiation (MJ/m^2/month), APAR is absorbed PAR (MJ/m^2/month), and FPAR is the Fraction of absorbed PAR, based on satellite data (See Section 3.2.). LUE (gC/MJ) represents the quantum efficiency of vegetation growth including environmental factors, and is generally described as LUE=LUEmax*Stress, derived from maximum LUE (LUEmax; gC/MJ) and a reduction of LUEmax due to environmental stresses (Stress) [e.g. Potter et al., 1993; Cramer et al., 1999]. The LUE concept has been applied in many existing models [e.g. Jarvis and Leverenz, 1983; Prince, 1991; Potter et al., 1993; Prince and Goward, 1995; Ruimy et al., 1994, 1996; Runyon et al., 1994; Running et al., 1999; Heinsch et al., 2003], and has been used to analyze interannual variations in NPP and NEP at the regional and global scale [Goetz et al., 2000; Potter et al., 2003; Nemani et al., 2003].

A large degree of uncertainty exists in estimating LUE values. Ruimy et al. [1999] demonstrated that the large differences in NPP estimates of existing biosphere models result from differences in LUE values used by those models. Two major problems in this regard are (i) accurately predicting the LUEmax value for each Plant Functional Type (PFT), and (ii) the simple and empirical calculation of stress factors, which lacks a biophysical and biochemical approach.

Although biochemical photosynthesis models [e.g. Farquhar et al., 1980; Farquhar and von Caemmerer, 1982; Collatz et al., 1991, 1992] describe the effect of air temperature, vapor pressure, soil water, and atmospheric CO_2 on photosynthesis, no existing LUE-based models provide a comprehensive account of these environmental stresses. For example, Monteith [1977] and Ruimy et al. [1994] did not include any stress factors in their formulations, while Ruimy et al. [1996], Prince and Goward [1995], and Heinsch et al. [2003] included only air temperature and vapor pressure. Potter et al. [1993] calculated stress factors empirically from air temperature and evapotranspiration. To improve the accuracy of GPP estimates that employ the LUE concept, it is necessary to develop a more comprehensive

theoretical model that incorporates stress factors that reflect biochemical and biophysical photosynthesis processes.

In the current paper, we propose a new Stress calculation method for the LUE concept based on a photosynthesis model and stomatal formulation. We call this model the Biosphere model integrating Eco-physiological And Mechanistic approaches using Satellite data (BEAMS), and evaluate the model on a global scale by comparing our results with those of existing biosphere models. We use our model, including the stress calculation, to simulate spatial and temporal variations in NPP and NEP at a global scale over the past two decades, and use sensitivity analysis to evaluate the primary mechanisms of change in NPP and NEP.

2. Description of BEAMS

BEAMS consists of hydrological and carbon cycle submodels, including the Stress calculation (Figures 1 and 2); these two submodels are linked as required during the simulation. The temporal resolution is monthly, and spatial resolution is 1*1 degree. The Stress calculation and two submodels are described in the following sections, while parameters used in the calculations are listed in Table 1.

2.1. Definition of Stress

Photosynthesis activities have a large effect on terrestrial carbon fluxes, and are in turn affected by environmental factors such as light, temperature, water, CO_2 and nitrogen. In the present study, we developed a new stress approach for the LUE concept, defining interaction using biophysical and biochemical equations. As temperature and water factors play an important role in plant growth activity, we focus on the effects of temperature and water on GPP. These two factors can generally be expressed using the three parameters of soil water, vapor pressure and air temperature. We calculate Stress from all three parameters, applying the biophysical responses of photosynthesis using a photosynthesis model coupled with a stomatal conductance formulation [Farquhar et al., 1980; Collatz et al., 1991; Ball et al.,

1987; Leuning, 1990]. Upscaling from leaf to canopy is based on the big-leaf approach. This method of calculation provides a more realistic Stress estimate, and accommodates interaction between all environmental factors.

We define Stress as the ratio of actual to maximum photosynthesis (P_{actual} and P_{max} in μmol/m^2/s) based on a photosynthesis rate (Figure 1), which accounts for the biochemical responses of temperature, relative humidity, and soil water content:

$$\text{Stress} = \frac{P_{actual}}{P_{max}} = \frac{P(\text{temp}, \text{hs}, \text{Fsoil1}, \text{Fsoil2})}{P(\text{temp_}_{opt}, \text{hs_}_{opt}, \text{Fsoil1_}_{opt}, \text{Fsoil2_}_{opt})} \quad (2)$$

where temp, hs, and Fsoil are temperature, relative humidity, soil water status, respectively. Relative humidity is derived from vapor pressure and air temperature using Tetens's equation. P_{actual} and P_{max} are calculated using the given and optimum climate conditions of temperature (temp and temp$_{}_{opt}$), relative humidity (hs and hs$_{}_{opt}$) and soil water status (Fsoil1, Fsoil2, Fsoil1$_{}_{opt}$, and Fsoil2$_{}_{opt}$). Maximum photosynthesis (P_{max}) is calculated using the optimum temperature (temp$_{}_{opt}$ is calculated by an iterative computation, in which temperature values are varied from 0 to 35 degC), optimum humidity (hs$_{}_{opt}$ = 100%), optimum soil water status for the maximum rate of carboxylation (Fsoil1$_{}_{opt}$ = 1.0), and optimum soil water status for stomatal conductance (Fsoil2$_{}_{opt}$ = 1.0), which maximizes the photosynthesis rate at a given condition.

2.2. Photosynthesis model and stomatal conductance formulation

Photosynthesis rate is calculated from climate parameters via a photosynthesis model and stomatal conductance formulation. Biophysical and biochemical parameters used in these equations are described in Table 1-1. Temperature-dependent parameters are Kc, Ko, Vcmax, and τ, while Vcmax and Gst are water-dependent. The photosynthesis rate (P) is described by the following equation:

$$P = \min\{Pl, Ps, Pm\} \quad (3)$$

where Pl, Ps, and Pm are potential photosynthesis rates (μmol/m^2/s). The above equation shows that C3 species are expressed as the minimum of the three potential capacities to fix carbon following the simplified Farquhar's equations [Farquhar et al., 1980; Collatz et al., 1991; De Pury and Farquhar, 1997]. Pl, Ps, and Pm are given by the following equations;

$$Ps = \frac{Vcmax * (pi - \Gamma_*)}{pi + Kc * (1.0 + O_2 / Ko)} \quad (4)$$

$$Pl = \frac{J * (pi - \Gamma_*)}{4.0 * (pi + 2.0\Gamma_*)} \quad (5)$$

$$Pm = 0.5 * Vcmax \quad (6)$$

Kc and Ko are dependent on temperature [Collatz et al., 1991], while Vcmax varies with temperature and soil moisture:

$$Kc = Kc_{25} * Q_{10Kc}^{(temp-298.15)/10.0} \quad (7)$$

$$Ko = Ko_{25} * Q_{10Ko}^{(temp-298.15)/10.0} \quad (8)$$

$$Vcmax = Vcmax_{25} * Q_{10Vcmax}^{(temp-298.15)/10.0} * Fsoil1 \quad (9)$$

where $Vcmax_{25}$ is defined for each PFT [Wullschlenger, 1993], and Q_{10Kc}, Q_{10Ko}, and $Q_{10Vcmax}$ are given by Collatz et al. [1991]. Fsoil1 is given by the following equation [Sellers et al., 1996]:

$$Fsoil1 = \frac{1.0}{1.0 + \exp(0.02 * (\Psi wp - \Psi))} \quad (10)$$

where Ψwp and Ψ are calculated by the hydrology submodel (Section 2.4.). Ψ represents the relative quantity of the soil water and is one of the essential environmental factors that affect plant photosynthetic activity. Ψ was calculated from the volumetric soil moisture (V), as follows:

$$\Psi = \Psi s * V^{-B} \tag{11}$$

where Ψs and B are defined for each soil type [Zobler, 1986]. $\Gamma *$ is given by

$$\Gamma * = \frac{P_atm * Oxy}{2.0 * \tau} \tag{12}$$

where τ is dependent on temperature:

$$\tau = \tau_{25} * Q_{10tau}^{(temp-298.15)/10.0} \tag{13}$$

J is required in equation (5), and is calculated from the following equation [De Pury and Farquhar, 1997]:

$$\theta_j * J^2 + (Jmax + I_j) * J + Jmax * I_j = 0 \tag{14}$$

where I_j is dependent on downward short wave radiation. Finally, the leaf net assimilation rate, Pn, is given by

$$Pn = P - Rd \tag{15}$$

where Rd is proportional to Vcmax [Sellers et al., 1992, 1996].

The relationship between photosynthesis rate (Pn) and CO_2 pressure in intercellular space (pi) is expressed by a diffusion equation:

$$Pn = \frac{G * (patm - pi)}{P_atm} \tag{16}$$

Where G is the total conductance to CO_2, given as:

$$1.0 / G = 1.0 / Gst + 1.0 / Gbl \tag{17}$$

where Gbl is calculated from wind speed, the zero plane displacement, surface roughness, and the Karman constant [Monteith, 1965]. The value of Gst is calculated from the equation of Ball et al. [1987], as adopted by Leuning [1990]:

$$Gst = 1.0 / 1.6 * \left(b + \frac{m * hs * Pn}{(patm - \Gamma)} * Fsoil2 \right) \tag{18}$$

where b and m are assumed as universal constant values (= 0.01, 9.2). The soil water stress for stomatal conductance (Fsoil2) is calculated from the following equation [Hanan and Prince, 1997]:

$$Fsoil2 = \frac{\Psi - \Psi wp}{\Psi fc - \Psi wp} \tag{19}$$

where Ψfc and Ψwp are defined for each soil type.

2.3. Carbon cycle submodel

The carbon cycle submodel consists of three biomass pools, four litter pools, and

five components of soil organic matter pools, with four carbon fluxes of GPP, autotrophic respiration (Ra), litter fall (LF), and soil decomposition (SD; Figure 2). NPP is defined as the carbon flow of GPP minus Ra (NPP = GPP - Ra). We modeled GPP based on the LUE concept using a satellite-based monthly FPAR data set and stress calculation, while other carbon pools and fluxes were modeled mechanically. Phenology is expressed on the basis of satellite-based FPAR and Leaf Area Index (LAI) as seasonally variable inputs. SD modeling is based on the carbon cycle component of the Century model [Parton et al., 1993].

The GPP calculation is based on the LUE concept including Stress calculated in the photosynthesis model (see equation (1) and Section 3.2.), which takes into account the environmental effects of air temperature, relative humidity, soil moisture, and atmospheric CO_2 concentrations on vegetation growth. GPP is allocated into leaf, stem, and root components by an empirical equation using climate parameters [Friedlingstein et al., 1999].

The Ra of leaf, stem, and root ($Ram_{leaf, stem, root}$) consists of maintenance and growth respiration. Maintenance respiration (Ram) is modeled in proportion to biomass with temperature dependence [McGuire et al., 1992; Heinsch et al., 2003], and growth respiration (Rag) is modeled in proportion to the potential NPP (=GPP - Ram) [Raich et al., 1991], as follows:

$$Ram_{leaf, stem, root} = kr_{leaf, stem, root} * Cbio_{leaf, stem, root} * Q10function \quad (20)$$

$$Rag_{leaf, stem, root} = fr_g * (GPP_{leaf, stem, root} - Ram_{leaf, stem, root}) \quad (21)$$

where $kr_{leaf, stem, root}$ is the specific respiration rate of leaf, stem, and root [Heinsch et al., 2003], and $Cbio_{leaf, stem, root}$ is the carbon mass of leaf, stem and root. Only $Cbio_{leaf}$ is calculated using LAI and Specific Leaf Area (SLA) defined for each PFT [Heinsch et al., 2003]. The Q10 function is the temperature dependence of maintenance respiration (Q10 = 2.0).

The LF of stem and root ($LF_{_stem,\ root}$) are assumed to be proportional to stem and root biomass, respectively (Ito and Oikawa, 2002). Leaf LF ($LF_{_leaf}$) is calculated from $Cbio_{_leaf}$ of the previous and current months. Each litter fall is calculated as

$$LF_{_stem,\ root} = kl_{_stem,\ root} * Cbio_{_stem,\ root} \quad (22)$$

$$LF_{_leaf} = NPP_{_leaf} - (Cbio_{_leaf}(t) - Cbio_{_leaf}(t-1)) \quad (23)$$

where $kl_{_stem,}$ $kl_{_root}$ are the specific litter fall rate of stem and root, respectively. LF is divided into structural and metabolic plant material based on the ratio of lignin to nitrogen (LN), defined as a constant for each PFT (Fm = 0.99 - 0.0018*LN; Fm is a fraction of metabolic litter fall). $LF_{_leaf}$ and $LF_{_stem}$ are metabolic and structural surface litter, respectively, and $LF_{_root}$ is metabolic and structural root litter, following Parton et al. [1993].

The SD submodel is based on the carbon cycle component of the CENTURY model [Parton et al., 1993], and describes the major soil carbon pools and transformation processes that connect them at the ecosystem level. The model comprises four litter carbon pools and five soil organic matter pools (SOMs; Figure 2).

The structural and metabolic $LF_{_leaf}$ and $LF_{_stem}$ are absorbed into "surface structural C" and "surface metabolic C", respectively, as inputs into the SD submodel. The structural and metabolic $LF_{_root}$ are absorbed into "root structural C" and "root metabolic C", respectively. SD is proportional to each litter or soil carbon pool size, and is affected by differences in each PFT and soil type, including water and temperature dependences. Carbon fluxes (Cflow) from each soil reservoir are calculated by:

$$Cflowi = k_i * Lc * Cs_i * D_{tw} * (1 - M_i) \quad i = 1,2 \quad (24)$$

$$Cflowi = k_i * Tm * Cs_i * D_{tw} * (1 - M_i) \quad i = 3 \quad (25)$$

$$Cflowi = k_i * Cs_i * D_{tw} * (1 - M_i) \quad i = 4, 5, 6, 7, 8 \quad (26)$$

where k_i is the maximum decay rate constant for each soil carbon pool (/month); Cs_i is the carbon content of litter or SOM pool (gC/m^2; 1: surface structural C, 2: root structural C, 3: soil microbe, 4: surface microbe, 5: surface metabolic C, 6: root metabolic C, 7: slow C, 8: passive C, and 9: leached C); M_i includes the effect of soil type and soil water flow, while carbon transfer to microbial pools is estimated as a fraction of M_i instead of 1-M_i; D_{tw} depends on soil water content and temperature, and only the temperature dependence of D_{tw} is modified using a Q_{10} function; and Tm is calculated from the silt plus clay fraction [Parton et al., 1993].

2.4. Hydrological submodel

The hydrological submodel is based on the BIOME3 model [Haxeltine and Prentice, 1996], and includes three water pools and six water fluxes. The water pools consists of a surface snow pack pool, and two layers at depths of 0-500 mm and >500 mm, defined for each soil type. The fluxes represent precipitation, evaporation, transpiration, snowmelt, percolation from the upper to lower soil layer, and run-off from soil water pools (overswell from soil bucket pools).

The soil water content (W_1, W_2) is given by the equations below. Only the field capacity (FC) and wilting point (WP) limit the maximum and minimum soil water content, and are defined for each soil property [Saxton et al., 1986].

$$\frac{dW_1(t)}{dt} = PPT(t) - \beta_1 \cdot EET(t) - Perc(t) - runoff_1 \quad (27)$$

$$\frac{dW_2(t)}{dt} = Perc(t) - \beta_2 \cdot EET(t) - runoff_2 \quad (28)$$

where β_1 and β_2 are derived from the soil water content and a root fraction for each soil layer ($\beta_1 + \beta_2 = 1.0$) [Haxeltine and Prentice, 1996], Perc is the percolation determined from

the empirical equation based on Darcy's law [Neilson, 1995], and PPT is water flux into the soil, including snowmelt. For monthly average air temperatures (Temp) of <0 degC, precipitation is stored in the snow pack pool, and PPT = 0. Snowpack is added to PPT in the first month when temp >0 [Potter et al., 1993, Parton et al., 1993]. The estimated evapotranspiration (EET; mm/month) is given by an empirical method [Potter et al., 1993]:

$$EET(t) = \min\{ PPT(t) + (PET(t) - PPT(t))*RDR, PPT(t) + (W_1(t-1) - WP) \} \quad \text{(For PPT < PET)} \quad (29)$$

$$EET(t) = PET(t) \quad \text{(For PPT} \geq \text{PET)} \quad (30)$$

where RDR is calculated using an empirical equation based on the relationship between the soil water potential and volumetric moisture content [Saxton et al., 1986; Potter et al., 1993]. The potential evapotranspiration (PET) is obtained using the Penman-Monteith method, which requires inputs of soil temperature (Ts), and stomatal resistance (rs). Ts is calculated as the soil temperature at the top of each soil layer using soil thermal diffusivities, air temperature, and soil water content [Campbell and Norman, 1998; Sitch et al., 2003]. Stomatal resistance is calculated from the photosynthesis model and conductance formulation (see Section 2.2.).

3. Input data

Table 2 summarizes the input data sets used in this study. All input data sets were re-sampled to a 1-degree spatial resolution for conformity with the vegetation map. Details of the input data sets are described in the following sections.

3.1. Climate data

The climate parameters used in our analysis were precipitation (Prec, mm), air temperature (Temp, degC), vapor pressure (VP, hPa), incoming surface solar radiation (SOL,

W/m^2), net surface short/long wave radiation flux (NSW/NLW, W/m^2), and wind speed (WND, m/s). Values of Prec, Temp and VP are sourced from the Climatic Research Unit (CRU) TS 2.0 data-set [Mitchell et al., 2003], which covers the period of 1901-2000 with a spatial resolution of 0.5 degrees lat/longitude and a monthly temporal resolution. SOL, WND, NSW and NLW were derived from the the National Centers for Environmental Prediction and National Center for Atmospheric Research (NCEP/NCAR) reanalysis data set, and were converted from daily to monthly temporal resolution. Atmospheric CO_2 concentrations are sourced from monthly observation records at Mauna Loa [Keeling and Whorf, 2002], and assumed to be representative of global values.

3.2. Satellite-based FPAR and LAI data

We used FPAR and LAI data sets based on the Normalized Difference Vegetation Index (NDVI) of the Global Inventory Monitoring and Modeling Studies (GIMMS). FPAR and LAI were obtained using a canopy radiative transfer model [Myneni et al., 1997a; Nemani et al., 2003]. The data set covers 1981 to 2002 with a temporal resolution of one month and spatial resolution of 0.5 degrees.

3.3. Land Cover Map, Soil and Elevation data

We used the NDVI-derived land cover map of Defries and Townshend [1994], which classifies vegetation types into 11 classes: broadleaf evergreen forest, coniferous evergreen forest and woodland, high latitude deciduous forest and woodland, tundra, mixed coniferous forest and woodland, wooded grassland, grassland, bare ground, shrubs and bare ground, cultivated crops, and broadleaf deciduous forest and woodland. Soil texture data from the United Nations Food and Agriculture Organization (FAO) and NASA's Goddard Institute for Space Studies (GISS) data sets [Zobler, 1986] were used and physical soil parameters such as volumetric water content and field capacity were estimated using the techniques of Cosby et al. [1984]. Soil profile depth is from Webb et al. [1993]. Elevation was derived from the U.S. Navy Fleet Numerical Oceanography Center (FNOC) 10-minute elevation data set [Cuming

et al., 1981]. Elevation data were used only for the calculation of atmospheric pressure.

4. Experiment

BEAMS-derived GPP estimates were evaluated using observed GPP values (see Section 5.1.). First, we evaluated the seasonal variation in GPP for an 8-year period from 1992 to 1999 using inventory data from the Harvard Forest, a deciduous broadleaf forest located at 42°32'21.6"N, 72°10'40.6"W. Following this, annual GPP values were calculated using the same method for 16 flux sites in Europe and North and South America, and these annual GPP values were evaluated against annual GPP values observed at flux site. BEAMS simulates GPP at a point scale and temporal resolution of one month (our_GPP). Assuming that the terrestrial carbon cycle at each flux site was in equilibrium during the first year of the simulation, we ran the model until NEP reached an equilibrium state. GPP was estimated from meteorological data (e.g. solar radiation, vapor pressure) and FPAR based on satellite observations. The meteorological parameters required by the LUE concept were obtained from meteorological data measured at the flux site [Falge et al., 2001a, 2001b]. FPAR data were sourced from FPAR data sets based on GIMMS [Myneni et al., 1997a; Nemani et al., 2003]. To compare our estimates with those of other studies, additional GPP values were calculated using the MOD17/GPP algorithm from the same inputs (mod_GPP). Our_GPP and mod_GPP were evaluated using GPP based on the Net Ecosystem Exchange of CO_2 (NEE) as measured at each flux site (flux_GPP). Flux_GPP was calculated from nighttime and total NEE using the Q10 function. Measured NEE data were based on gap-filled flux data [Falge et al., 2001a, 2001b], while Q10 values were sourced from previous studies [e.g. Hollinger et al., 1999; Boone et al., 1998; Law et al., 1999].

BEAMS was used to simulate terrestrial carbon fluxes and pools on a global scale with 1-degree spatial resolution and a monthly temporal resolution (Section 5.2. to 5.5.). Assuming that the terrestrial carbon cycle was in equilibrium during 1982, we first ran the

model until NEP reached an equilibrium state using 1982 climate, atmospheric CO_2, and LAI and FPAR data. On the basis of the equilibrium status, BEAMS was operated from 1982 to 2000 using climate, atmospheric CO_2, and LAI and FPAR time-series data.

Stress factors were simulated using our Stress approach (Section 5.2.). Stresses caused by temperature and water factors were simulated independently by alternately fixing water (Stress_w) and temperature (Stress_t) status as optimal to evaluate temperature and water stress separately. Spatial variation in Stress was also calculated via the CASA model [Potter et al., 1993] and MOD17 product [Heinsch et al., 2003] to enable comparison with BEAMS data. CASA-derived Stress is modeled empirically using two temperature factors and one water factor. CASA-derived Stress_t is modeled to account for (1) large respiration costs for cold and hot environments (equation (6) in Potter et al. [1993]), and (2) the reduction in light use efficiency at temperatures above and below the optimum (equation (7) in Potter et al. [1993]). CASA-derived Stress_w is modeled using estimated and potential evapotranspiration within the range 0.5-1.0 (equation (8) in Potter et al. [1993]). MOD17-derived Stress includes the effects of temperature and vapor pressure deficit determined using a linear function, while setting the temperature and vapor pressure deficit at Stress = 1.0 (optimum conditions) and Stress = 0.0 (no growth). The Stress factors in CASA and MOD17 were calculated using the same input data sets (Section 3.).

We evaluated the simulated annual average NPP values from 1982 to 2000 with data from the IGBP-DIS Global Primary Production Data Initiative (GPPDI) [Zheng et al., 2003] (Section 5.3.). The GPPDI data set was obtained from the Oak Ridge NPP database as observational NPP data, and contains 2335 cells based on observational and modeling data. We extrapolated or regionalized the higher quality data sets to grid cell sizes of up to 0.5 * 0.5 degrees; we used data resampled to 1 * 1 degree (pixel values were averaged from half-degree data).

We calculated a linear trend in NPP from 1982 to 2000, and analyzed the factors that

influenced this trend (Section 5.4.). We estimated the linear trend in NPP based on time-variable climate data and satellite-based LAI and FPAR data (default-run). To understand the mechanisms of the NPP trend, we analyzed the sensitivity of the NPP trend to variation in different input variables (climate parameters, vegetation data based on the satellite observation, or atmospheric CO_2) while other variables were held constant at their 1982 monthly values over the period 1982 to 2000.

Inter-annual variations in NEP, and the mechanisms responsible for these variations, were analyzed on a global scale from 1983 to 2000 (Section 5.5.). Higher NEP anomalies indicate an increase in carbon uptake by the biosphere, while lower values indicate increased carbon release. A default-run was first conducted with time-variable climate and FPAR and LAI data. A sensitivity analysis was performed for each input variable to determine the effect of climate and vegetation parameters on inter-annual NEP variations. We varied successive input variables over the period 1982 to 2000, while all other variables were held at their 1982 monthly values. NEP, which in 1982 was largely affected by spin-up, was not considered in this analysis.

5. Results and Discussion

5.1. Comparison of GPP with flux site data

The first result is a comparison of modeled and observed seasonal GPP variation (Figure 3). Our_GPP data shows a better fit to flux_GPP than that achieved by mod_GPP. By improving the Stress calculation, we achieved a better correspondence, in absolute values, between our_GPP and flux_GPP, indicating that our_GPP data are more accurate than mod_GPP. In terms of detecting the growing season and leaf drop season, the accuracy achieved in describing the two seasonal changes indicates a strong correspondence with flux_GPP, as both our_GPP and mod_GPP have a strong dependence on FPAR. For the summer season, our_GPP values are reasonable, but mod_GPP values were clearly

underestimated. These results indicate that seasonal variation in GPP is more accurately calculated using our new Stress approach. In the future, BEAMS will be used to simulate GPP for the years from 2000 using MODIS/FPAR data sets, and the results will need to be evaluated by comparison with observational data.

Our second result is a comparison of mod_GPP, our_GPP and flux_GPP (Figure 4, Table 3). We found that our_GPP produced a stronger correlation with GPP measurements at more flux sites than that achieved by mod_GPP. Both our results and MOD17 results contain a slight overestimation, but the correlation coefficient for our estimate (R^2=0.76) was stronger than that for the MOD17 estimate (R^2=0.47). We conclude that our estimates are in good agreement with observational data at the flux sites in terms of seasonal changes and annual absolute GPP values. The differences between our_GPP and flux_GPP shown in Figure 4 are larger than those shown in Figure 3, because annual GPP values include the accumulated errors involved in the monthly GPP values. We conclude that the errors result not only from our estimation method, but also include errors involved in the calculation of GPP from observed NEE, errors in the observation equipment, and errors resulting from observation conditions. In the future, the accuracy of our GPP calculations will be improved by calibrating vegetation parameters defined for each PFT.

5.2. Spatial distribution of modeled Stress

We calculated the spatial distribution of annual average water and temperature stresses (Stress), Stress_t, and Stress_w by BEAMS for 1982-2000 (left-hand image in Figure 5). High Stress values were recorded for eastern North America, temperate South America, central Africa and parts of Southeast Asia, while low Stress readings were recorded for high latitudes and semi-desert areas. Stress_t values were lower than Stress_w in some areas. In the Amazon area, the Stress factor was limited more by temperature (Stress_t = 0.81-0.88, Stress = 0.74-0.80) than by lack of water or dryness (Stress_w = 0.92-0.98). This indicates that the limitations on plant activity related to air temperature are greater than the limitations due to

water availability or the effect of high temperature stress. The stresses recorded in central Africa and parts of Southeast Asia showed similar trends. Values of Stress_t in tundra areas were low (Stress_t = 0.08-0.13, Stress_w = 0.23-0.30, Stress = 0.06-0.12), indicating that plants in cold conditions were affected by low temperature stress. Temperature conditions were optimal for plants in tropical and temperate semiarid regions such as southern and northern Africa, parts of western North America, Australia, and China.

The highest Stress values were recorded in the equatorial regions, and these values decrease toward higher latitudes and in drier regions (upper images in Figure 5). The three different models used in this study produced contrasting Stress values in certain areas. In equatorial regions, the highest Stress was produced by MOD17 (0.95-0.99), while CASA produced intermediate values (0.85-0.93), and BEAMS produced the lowest values (0.74-0.83). In Europe, MOD17 generated the highest Stress values (0.72-0.85), followed by BEAMS (0.42-0.82) and CASA (0.39-0.63). In parts of Western Europe, the BEAMS and MOD17 Stresses are similar, but in other areas the BEAMS values are similar to those generated by CASA. In parts of western North America, BEAMS Stress values are lowest and MOD17 values highest, while in eastern North America, the CASA Stress values are lowest and those of MOD17 highest. In northwest China, the MOD17 Stress values are highest and the BEAMS values lowest (0.07-0.42).

Values of Stress_w are high in humid tropical and temperate regions, and decrease toward drier regions. The BEAMS Stress_w values generally differ from values derived from the other models (lower images in Figure 5); BEAMS Stress_w values for middle and high latitudes are lower than MOD17 and CASA values. MOD17 Stress_w values are generally highest, especially at high latitudes, while BEAMS values are generally lowest in these regions. We consider the MOD17 and CASA values to be anomalously high due to problems in the calculation methods of the models. For example, MOD17 uses only vapor pressure deficit, and does not account for the water stress derived from soil moisture. In CASA,

calculated Stress_w values were >0.5 for every cell, even for dry semi-desert areas. Stomatal behavior is sensitive to vapor pressure, and as saturate vapor pressure is low in low temperature conditions, stomata are likely respond to such conditions with a water deficit. It seems unlikely that the vapor pressure was close to saturation for the entire year. The MOD17 and CASA models need to be reevaluated and their accuracy improved, as well as being made easier to use. We recommend that estimates of water stress should be based increasingly on biophysical responses.

BEAMS-derived Stress_t for equatorial and high latitude regions is lower than that derived from the MOD17 and CASA models, but the three Stress_t patterns are similar (middle image, Figure 5). Considering the values of Stress_w, air temperature is a dominant factor influencing the determined Stresses, however, the degree of dependence on Stress_w and Stress_t differs between the three models. At high latitudes, all three Stress_t values (0.06-0.41 for BEAMS, 0.12-0.28 for CASA, 0.24-0.32 for MOD17) are larger than Stress_w values (0.46-0.05, 0.81-0.95, 0.97-1.0), although the difference between BEAMS Stress_t and Stress_w is relatively small. In semi-desert areas such as northwest China, CASA and MOD17-derived Stress_t is significantly lower than Stress_w, but our results produce similar values of Stress_w and Stress_t. For global Stress values therefore, the effect of air temperature on plant activity is greater than the effect of water conditions such as vapor pressure and soil water, however, the biophysical stress approach has identified that water stress is an important factor in photosynthesis activity. In dry areas such as northwest China, water stress is as important a factor as temperature stress.

In equatorial regions, the Stress_t component of BEAMS Stress was larger than the Stress_w component, whereas for CASA and MOD17 this trend was reversed. This pattern is explained by the fact that BEAMS Stress_t is limited by the effect of interaction between water and temperature stresses and high temperature stress. In considering such interaction, our two Stress calculations might not be appropriate, as they are expressed only as a simple

multiplication. In addition, Stress_t was calculated using uncritical equations. For example, in MOD17, higher air temperatures result in higher Stress_t values. In CASA, the calculation of stress equations involved fitting two curves, while parameters were determined empirically or arbitrary. In reality, photosynthesis activity is limited by temperature in excess of optimum conditions, and response curves are different for different environmental conditions (e.g. PFT, soil type, solar radiation, soil water content). We recommend that Stress calculations include a more accurate account of temperature response. BEAMS, CASA, and MOD17 Stress values are high for equatorial regions, indicating that an understanding of these regions is important for our understanding of global carbon fluxes, and that we need to calculate Stress more accurately.

We have demonstrated that our BEAMS results differed markedly from the results of the CASA and MOD17 models. In the areas where the predicted Stress values of the three models are different, we should carefully consider the effect of environmental stresses on photosyntesis activity. Our simplified and more accurate Stress approach enabled the estimation of GPP from satellite data. The Stress calculations used in the present study represent a significant advance over those of other models, as we employ biophysical photosynthesis models. However, there is room for improvement in our Stress calculation method; biophysical parameters and processes used in the model contain an element of uncertainty (e.g. the relationship between soil water and photosynthesis activity, and photosynthesis processes in C4 species). In terms of the relationship between soil water and photosynthesis rate, equations (10) and (19) are embedded empirically, and there exists room for improvement in this regard. Understanding of these biophysical processes is important for carbon cycle research, and we need to further clarify the mechanisms of photosynthesis activity and stomatal behavior. These mechanisms should then be incorporated into carbon estimates.

5.3. Spatial distribution of NPP and comparison with GPPDI database

The spatial variation in annual NPP averaged for the period 1982-2000 is a reasonable representation of climate effects (e.g. air temperature, precipitation) on plant growth [e.g. Cramer et al., 1999] (Figure 6). High NPP values occur over the tropical forest regions, and generally decrease at higher latitudes. High NPP values, above 1200 gC/m^2/yr, are obtained for eastern North America, Amazon basin, central Africa, and parts of Southeast Asia. In contrast, low NPP values are found in the desert regions and at high latitudes. Global NPP values determined by BEAMS are 54.9 GtC/yr averaged for the period 1982-2000, which is within the range of estimates made in previous studies [Cramer et al., 1999].

The correlation coefficient for average BEAMS NPP over 19 years compared with the GPPDI database is 0.86 (Figure 7). The BEAMS estimates are slightly higher than the GPPDI database, but a NPP pattern for each PFT is adequately estimated. For example, the highest NPP value was in broadleaf evergreen forest, while NPP in grassland was lower than in forests. The BEAMS correlation coefficient is significantly higher than the value obtained for the Miami model (R^2 = 0.73; Zheng et al. [2003]). We therefore conclude that the spatial patterns and absolute NPP values for each PFT generated by BEAMS are reasonable. In the future, we need to consider the vegetation parameters defined for each PFT. Observed or measured NPP values generally include some uncertainties, such as empirical approximations and scaling issues, and it would be difficult to evaluate NPP values in greater detail than that attempted in the present analysis.

5.4. NPP trend analysis using a sensitivity study of input parameters

NPP increased in most regions (e.g. Northern mid-latitudes, high latitudinal zones, and equatorial regions) from 1982 to 2000 (Figure 8). Marked NPP increases in excess of +10 gC/m2/yr were recorded in the Amazon, Europe, eastern North America, equatorial Africa, and Russia. In contrast, decreases in NPP in excess of –10 gC/m^2/yr were recorded in Southeast Asia, central Africa, and Canada. The greatest changes in NPP occurred in the northern mid-latitudes and high latitudes of Europe and eastern North America, equatorial

areas of the Amazon, southern Africa, and Southeast Asia ($p < 0.05$; p is the significance level of the linear trend).

By isolating these NPP trends to identify the effects of independent input parameters, we found that temporal variations in FPAR, air temperature, precipitation, vapor pressure, radiation (downward short wave radiation and net short and long wave radiation), wind speed, and atmospheric CO_2 have significant effects on the NPP trends (Figure 9). To confirm the effect on NPP trends of the rate of annual change in 8 time-series inputs, we also calculated the spatial variation in the change rates as a supplement to the trend analysis (Figure 10). The effects of each parameter on the NPP trends are as follows: (1) temperature increase (e.g. northern North America, Amazon, Southeast Asia, Siberia) generates a negative BEAMS NPP trend due to increases in autotrophic respiration; (2) changes in precipitation and wind speed generally result in both increased and decreased NPP in several regions; (3) changes in vapor pressure result in positive NPP trends in northern mid-latitudes and high latitudinal areas; (4) increases in radiation result in positive trends in the Amazon; (5) increases in CO_2 concentration generate positive NPP trends in equatorial areas, Europe, and eastern North America, and (6) FPAR results in positive trends in northern mid-latitudes and high latitudinal regions and the Africa Sahel region, and negative NPP trends in equatorial Africa, Canada, and parts of Southeast Asia. In contrast, temporal variations in LAI contribute to NPP increases in parts of Canada and in Siberian forest regions.

On the basis of the above results, the mechanisms of regional NPP trends can be characterized as follows: the observed NPP increase in the Amazon is mainly caused by an increase in radiation; in Europe, NPP increase results from increases in FPAR, radiation, and vapor pressure; in eastern Russia, increase in NPP results from increases in FPAR, vapor pressure, air temperature, wind speed, and precipitation; in southern North America increase in NPP results from increases in FPAR, vapor pressure, and radiation; in northern Africa increase in NPP results from increases in FPAR and precipitation; and in Australia increase in

NPP results from increases in FPAR and precipitation. In terms of decreases in NPP, the decrease in central Africa is caused by decreases in precipitation, radiation, and FPAR; in parts of Southeast Asia the decreases in NPP are related to decreases in radiation, FPAR, precipitation, and wind speed; and in Canada by air temperature, wind speed, precipitation, radiation, and FPAR decreases. The NPP increase recorded in northern mid-latitudes and high latitudes and the Amazon is consistent with the results of previous studies. Many previous papers report that terrestrial plants in the northern mid-latitudes and high latitudes have increased in activity with global warming [e.g. Myneni et al., 1997b; Lucht et al., 2002], and our results demonstrate that NPP increases in some of these areas were caused by changes in air temperature. Nemani et al. [2003] documented an increase in NPP in the Amazon area due to solar radiation increase over the period 1982-2000; we obtained similar results.

The BEAMS-derived NPP trend and sensitivity to various input parameters differs to the results of Nemani et al. [2003], which comprise NPP trend analysis and sensitivity studies for vegetation (FPAR and LAI) and climate data. Nemani et al. [2003] calculated NPP using the same LUE concept as BEAMS, but Stress was calculated only from Vapor Pressure Deficit (VPD) and temperature via an empirical equation and stress parameterization [MOD17 algorithm of Heinsch et al., 2003]. Nemani et al. used the FPAR and LAI data sets derived from GIMMS, the Pathfinder AVHRR Land data set (PAL; Myneni et al. [1997]) as vegetation data, and NCEP/NCAR as climate data.

The NPP trends derived from our analysis differ from the results of Nemani et al. [2003] for several regions. Our trends of increasing NPP are larger for Europe (+6 to +11 $gC/m^2/yr$ by BEAMS, compared with +4 to +6 by Nemani et al. [2003]), and Russia (+7 to +10, compared with +4 to +8), while we obtained smaller increases in northeast Canada (-2 to –8, +2 to +8), and central Africa (-1 to –10, +8 to -6). To determine which input data sets produced these differences in NPP trends, we investigated the trend values from our sensitivity study. Sensitivity studies of changing vegetation data with constant climate data

("Vegetation" in Figure 9) show that the results of the two studies are largely similar (Figure S8 in supplementary file of Nemani et al. [2003]), although slight differences exist for equatorial Africa and Southeast Asia, and our results decreased more than those of Nemani et al. The reason for these similarities is that both vegetation data sets are based on NOAA/AVHRR satellite observations. In contrast, analysis of changing climate data with constant vegetation data ("Climate" in Figure 9) shows clear differences between the two NPP trends, especially for Russia, Canada, and central South America. The effects of climate data (except radiation) on these differences can be explained as follows. The NPP increase recorded for Russia is controlled by vapor pressure, precipitation, air temperature, and wind speed; the increase for Canada is controlled by air temperature, precipitation, wind speed and atmospheric CO_2 concentration; and for central South America by vapor pressure and precipitation.

Differences in the two NPP trends result from differences in the Stress calculation method, as the sensitivity analysis revealed that the result for changing climate data with constant vegetation data was vastly different from NPP trends for changing vegetation data with constant climate data. The above comparisons show that the extent of the effects of each parameter on NPP is quite different, as reflected in the differences in the Stress calculation. If NPP was estimated over a longer time period, these differences would have an even greater affect on NPP variations. The Stress calculation is important for considering time variations in NPP. In the future, we need to deal with Stress more carefully, and evaluate or confirm the accuracy of the environmental parameters.

5.5. Inter-annual variations in NEP

Inter-annual variation in global NEP was simulated using BEAMS, and the results compared with terrestrial carbon exchange via the inverse approach (Figure 11). Temporal variation in simulated NEP corresponds well with the results of Bousquet et al. [2000]. Our model consists of vegetation and soil components, allowing us to calculate NEP from NPP

and SD using a bottom-up approach. We compared our simulated NEP temporal variation with the global terrestrial carbon exchange estimated for inverse modeling using atmospheric CO_2 observations and atmospheric transport for 1983 to 1997: the top-down approach of Bousquet et al. [2000]). We found that temporal variation in estimated NEP is reasonably simulated by BEAMS for these periods. It should be noted that there remain uncertainties in the inverse modeling process (e.g., Gurney et al. 2002), and that future studies should continue to compare carbon exchanges described by the two different approaches.

The sensitivity studies clarified the relative contribution of climate data, vegetation data by satellite observations and each of the four input climate parameters to interannual variability in NEP (Figure 12). The three time variation trends presented in Figure 12(a) demonstrate that NEP variability is strongly controlled by both climate and vegetation data. Figure 12(b) shows the contribution of the four climate parameters. NEP is strongly controlled by air temperature and precipitation; an increase in atmospheric CO_2 concentration results in an increase in NEP.

Several processes within BEAMS are affected by soil water and precipitation (GPP, including the new Stress approach, productivity allocation and soil decomposition processes). Air temperature is also important because most processes in BEAMS include a temperature variable. Recent increases in atmospheric CO_2 concentrations, which the other LUE models do not accommodate, act to enhance NEP. Increases in atmospheric CO_2 concentrations during 1983-2000 resulted in an increased NEP of approximately + 0.12 GtC/18 years. CO_2 fertilization is important for plant growth activity, and needs to be taken into account for satellite-based NPP modeling.

Volcanic eruption events have a strong effect on terrestrial carbon exchange. NEP increased during 1992-93 (+0.56, +0.18 GtC/yr in 1992, 93), following the eruptions at Mt. Pinatubo in 1991. Volcanic eruptions affect simulated terrestrial carbon via the following processes: (1) temperature cooling due to stratospheric volcanic aerosols [e.g. Ingersoll, 1983;

Rampino and Self, 1984; Self et al., 1996] results in decreases in GPP, Ra and SD, and (2) apparent decreases in satellite-based NDVI related to scattering of stratospheric aerosol results in anomalously low FPAR and LAI [e.g. Myneni et al., 1997b; Lucht et al., 2002].

Only BEAMS, which used the FPAR and LAI data sets based on GIMMS data, includes an atmospheric correction for volcanic eruption. Sensitivity studies of our results show that the decreases related to climate data are clearly larger than those related to vegetation data (Figure 12a). Our results are consistent with several studies that show a large terrestrial carbon uptake following the Mt. Pinatubo eruption [e.g. Bousquet et al., 2000; Le Quere et al., 2000]. Figure 12(b) shows that the NEP decrease is largely influenced by air temperature. Air temperature affects Ra and SD levels more than GPP. Our simulation of the volcanic eruption event shows that the increase in terrestrial carbon sink resulted from a decrease in Ra and SD.

BEAMS-derived NEP estimates correspond well with results from the top-down approach and volcanic eruption events, indicating that BEAMS can simulate NEP as well as GPP and NPP. Sensitivity analysis demonstrated that NEP is most affected by precipitation and air temperature. Results of the hydrological submodel, in combination with the relationships between carbon and hydrological processes, indicate that precipitation is also important for NEP estimation, and that temporal variation in NEP is largely controlled by climate and vegetation data. These results highlight the importance of evaluating the precision and accuracy of input data sets. Recent studies show that increases in diffused radiation following volcanic eruptions might affect photosynthesis activity (e.g. Gu et al., 2003). Radiation processes in the BEAMS model may therefore be important in evaluating the effect of volcanic eruption on NEP. To analyze NEP variation more successfully, we should evaluate input data sets (e.g. compare the temporal patterns of climate parameters in different data sets), and further develop the structure of BEAMS.

6. Conclusions

In this study we proposed a more realistic method of calculating Stress using the LUE concept and based on a photosynthesis model; from this we established a new biosphere model (BEAMS) to estimate terrestrial NPP and NEP. The Stress value is defined more realistically as the ratio of actual and optimum photosynthesis rates using climate input variables of temperature, relative humidity, and soil water content. BEAMS is based on the water and carbon cycles, and requires climate and satellite-based vegetation parameters as model inputs. We used BEAMS to simulate terrestrial carbon fluxes on a global scale.

The biophysical approach of BEAMS produces a more realistic Stress estimate than that of other models. We demonstrated that the spatial distribution of BEAMS Stress values is different from that of the MOD17 and CASA models. For example, the BEAMS water stress is lower than that of the other models because of soil moisture stress in the middle and high latitudinal regions. We analyzed environmental stress on a biophysical basis, enabling carbon fluxes to be accurately estimated. To confirm that BEAMS data provide an advantage in calculating terrestrial carbon fluxes, we compared BEAMS GPP estimates with observational measurements from flux sites. We found that the absolute BEAMS GPP value and patterns of temporal variation are consistent with GPP measured at flux sites.

We used BEAMS to successfully simulate spatial NPP patterns by comparing measurements with the GPPDI database. Recent changes in NPP and NEP were also analyzed via BEAMS. Trend analysis of NPP showed that global NPP increased during 1983-2000. CO_2 fertilization effects, which are not accounted for in previous models, also affect the calculated increases in NPP, especially at low latitudes. Comparison of our results with Nemani et al. [2003] reveal that differences in the Stress calculation and related processes (i.e. CO_2 fertilization, high temperature and soil moisture stress) are the cause of different patterns in NPP trends predicted by the two models. In addition, our results show that NEP estimated via BEAMS corresponds with results from the top-down approach, and accommodates the

effects of volcanic eruption events. The BEAMS model therefore provides a reasonable estimate of NEP, as well as simulating GPP and NPP.

We conclude that BEAMS is an appropriate method for the estimation of spatial and temporal patterns in terrestrial carbon fluxes, however, two further improvements to the model are recommended. First, the accuracy of plant and soil model parameters, which are currently based on the results of previous studies, should be revised and improved for future studies. Improvements are also required in terms of the realistic reconstruction of ecosystem processes, especially litter fall, by considering plant structure patterns in the same way as the Dynamic Global Vegetation Model (DGVM) [e.g. Sitch et al., 2003]. We recommend the development of a plant structure analysis for vegetation carbon pools, and verification of model analyses of these components using inventory data.

The second area of potential improvement is that of data sets. Many climate data sets are currently available, including CRU, NCEP/NCAR, NCEP Department of Energy AMIP-II Re-analysis (NCEP/DOE), and the 40-year European Center for Medium range Weather Forecasting Re-Analysis project (ECMWF/ERA40). To estimate the accuracy of terrestrial carbon flux estimates, these data sets must be evaluated and better land surface data sets selected. Terrestrial carbon fluxes should be reevaluated based on these proposed improvements.

Acknowledgements

We would like to acknowledge A. Ito (Frontier Research Center for Global Change), K. Hikosaka (Tohoku University) and T. Hiyama (Nagoya University) for their valuable comments on biophysical, biochemical and hydrological processes. The first author would like to acknowledge the Japanese Society for the Promotion of Science (JSPS) and Asahi Breweries, Ltd for financial support. K. Ichii and R. Nemani were funded by the NASA EOS program. We are also grateful to the data set producers and their collaborators. The terrestrial carbon flux data estimated by the top-down approach was produced by P. Bousquet. The FLUXNET program is sponsored by the NASA/EOS Validation Program. It contributes to the CARBODATA and CARBOEUROFLUX projects of the European Union (supported by the EC's Fifth Framework Programme, R and TD contract CARBOEUROFLUX, contract no EVK2-CT-1999-0032), the AmeriFlux program (US Department of Energy's Terrestrial Carbon Program, and NIGEC Program), and the EUSTACH-LBA project.

References

Asrar, G., M. Fuchs, E.T. Kanemasu, and J.L. Hatfield (1984), Estimating absorbed photosynthetic radiation and leaf area index from spectral reflectance in wheat, *Agron. J.*, *76*, 300-306.

Bakwin, P.S., K.J. Davis, C. Yi, S.C. Wofsy, J.W. Munger, L. Haszpra, and Z. Barcza (2004), Regional carbon dioxide fluxes from mixing ratio data, *Tellus Ser. B*, *56*, 310-311.

Ball, J.,I. Woodrow, and J.A. Berry (1987), A model predicting stomatal conductance and its contribution to the control of photosynthesis under different environmental conditions, *Progress in photosynthesis*, *4*, 221-224.

Boone, R.D., K.J. Nadelhoffer, J.D. Canary, and J.P. Kaye (1998), Roots exert a strong influence on the temperature sensitivity of soil respiration, *Nature*, *396*, 570–572.

Bousquet, P., P. Peylin, P. Ciais, C.L. Quéré, P. Friedlingstein, and P.P. Tans (2000), Regional changes in carbon dioxide fluxes of land and ocean since 1980, *Science*, *290*, 1342–1346.

Campbell, J.S., and J.M. Norman (1998), *An Introduction to Environmental Biophysics*, *286*, Springer

Collatz, G.J., J.T. Ball, C. Grivet, and J.A. Berry (1991), Physiological and environmental regulation of stomatal conductance, photosynthesis and transpiration: A model that includes a laminar boundary layer, *Agric. For. Meteorol.*, *54*, 107-136.

Collatz, G.J., M. Ribas-Carbo, and J.A. Berry (1992), Coupled photosynthesis-stomatal conductance model for leaves of C_4 plants, *Australian J. Plant Physiol.*, *19*, 519-538.

Cosby, B.J., G.M. Hornberger, R.B. Clapp, and T.R. Ginn (1984), A statistical exploration of the relationships of soil moisture characteristics to the physical properties of soils, *Water Resour. Res.*, *20*, 682-690.

Cramer, W., D.W. Kicklighter, A. Bondeau, B. Moore III, G. Churkina, B. Nemry, A. Ruimy, A.L. Schloss and the participants of the Potsdam NPP Model Intercomparison. (1999), Comparing global models of terrestrial net primary production (NPP): overview and key results, *Global Change Biol.*, *5*, 1-15.

Cuming, M.J., and B.A. Hawkins (1981), TERDAT: The FNOC System for Terrain Data Extraction and Processing. Technical Report Mil Project M-254 (second edition). Prepared for USN/FNOC and published by Meteorology International Inc.

DeFries, R.S., and J.R.G. Townshend (1994), NDVI-derived land cover classification at global scales, *Int. J. Remote Sens.*, *15*, 3567-3586.

De Pury D.G.G., and G.D. Farquhar (1997), Simple scaling of photosynthesis from leaves to canopies without the errors of big-leaf models, *Plant Cell Environ.*, *20*, 537-557.

Falge, E., D.D. Baldocchi, R.J. Olson, P. Anthoni, M. Aubinet, C. Bernhofer, G. Burba, R. Ceulemans, R. Clement, H. Dolman, A. Granier, P. Gross, T. Grünwald, D. Hollinger, N.O. Jensen, G. Katul, P. Keronen, A. Kowalski, C. Ta Lai, B.E. Law, T. Meyers, J. Moncrieff, E. Moors, J.W. Munger, K. Pilegaard, Ü. Rannik, C. Rebmann, A. Suyker, J. Tenhunen, K. Tu, S. Verma, T. Vesala, K. Wilson, and S. Wofsy (2001a), Gap Filling Strategies for Defensible Annual Sums of Net Ecosystem Exchange, *Agric. For. Meteorol.*, *107*, 43-69.

Falge, E., D.D. Baldocchi, R.J. Olson, P. Anthoni, M. Aubinet, C. Bernhofer, G. Burba, R. Ceulemans, R. Clement, H. Dolman, A. Granier, P. Gross, T. Grünwald, D. Hollinger, N.O. Jensen, G. Katul, P. Keronen, A. Kowalski, C. Ta Lai, B.E. Law, T. Meyers, J. Moncrieff, E. Moors, J.W. Munger, K. Pilegaard, Ü. Rannik, C. Rebmann, A. Suyker, J. Tenhunen, K. Tu, S. Verma, T. Vesala, K. Wilson, and S. Wofsy (2001b), Gap Filling

Strategies for Longterm Energy Flux Data Sets, *Agric. For. Meteorol.*, *107*, 71-77.

Falge, E., D.D. Baldocchi, J. Tenhunen, M. Aubinet, P. Bakwin, P. Berbigier, C. Bernhofer, G. Burba, R. Clement, K.J. Davis, J.A. Elbers, A.H. Goldstein, A. Grelle, A. Granier, J. Guomundsson, D. Hollinger, A.S. Kowalski, G. Katul, B.E. Law, Y. Malhi, T. Meyers, R.K. Monson, J.W. Munger, W. Oechel, K.T. Paw, K. Pilegaard, U. Rannik, C. Rebmann, A. Suyker, R. Valentini, K. Wilson, and S. Wofsy (2002), Seasonality of ecosystem respiration and gross primary production as derived from FLUXNET measurements, *Agric. For. Meteorol.*, *113*, 53-74.

Farquhar, G.,S. von Caemmener, and J. Berry (1980), A biochemical model of photosynthesis CO_2 fixation in leaves of C3 species, *Planta*, *149*, 78-90.

Farquhar, G.D., and S. von Caemmerer (1982), Modelling of photosynthetic responses to environmental conditions. In: Lange OL, Nobel PS, Osmond CB, Ziegeler H eds, Physiological Plant Ecology. II. Encyclopedia of plant physiology, New Series, *12B*. Berlin: Spiringer-Verlag, 548-577.

Foley, J.A., I.C. Prentice, N. Ramankutty, S. Levis, D. Pollard, S. Sitch, and A. Haxeltine (1996), An integrated biosphere model of land surface processes, terrestrial carbon balance, and vegetation dynamics, *Global Biogeochem. Cycles*, *10*, 603-628.

Friedlingstein, P., G. Joel, C.B. Field, and I.Y. Fung (1999), Toward an allocation scheme for global terrestrial carbon models, *Global Change Biol.*, *5*, 755-770.

Goetz, S.J., S.D. Prince, J. Small, A.R. Gleason, and M.M. Thawley (2000), Interannual variability of global terrestrial primary production: reduction of a model driven with satellite observations, *J. Geophys. Res.*, *105*, 20077-20091.

Gu, L., Baldocchi D.D., S.C. Wofsy, J.W. Munger, J.J. Michalsky, S.P. Urbanski, and T.A. Boden (2003), Response of a deciduous forest to the Mount Pinatubo eruption: enhanced photosynthesis, *Science*, *299*, 2035-2038.

Gurney, K.R., R. M. Law, A. S. Denning, P. J. Rayner, D. Baker, P. Bousquet, L. Bruhwiler, Y.-H. Chen, P. Ciais, S. Fan, I.Y. Fung, M. Gloor, M. Heimann, K. Higuchi, J. John, T. Maki, S. Maksyutov, K. Masarie, P. Peylin, M. Prather, B.C. Pak, J. Randerson, J. Sarmiento, S. Taguchi, T. Takahashi and C.-W. Yuen (2002), 2001: Towards robust regional estimates of CO2 sources and sinks using atmospheric transport models, *Nature*, *415*, 626-630.

Hanan, N.P., and S.D. Prince (1997), Stomatal conductance of West Central Supersite vegetation in HAPEX-Sahel: measurements and empirical models, *J. Hydrol.*, *188-189*, 536-562.

Haxeltine, A., and I.C. Prentice (1996), BIOME3: An equilibrium terrestrial biosphere model based on eco-physiological constraints, resource availability and competition among plant functional types, *Global Biogeochem. Cycles*, *10*, 693-709.

Heinsch, F.A., M. Reeves, C.F. Bowker, P. Votava, S. Kang, C. Milesi, M. Zhao, J. Glassy, R.R. Nemani, and S.W. Running (2003), GPP and NPP (MOD17A2/A3) Products NASA MODIS Land Algorithm: *MOD17 User's Guide*

Hollinger, D.Y., S.M. Goltz, E.A. Davidson, J.T. Lee, K. Tu, and H.T. Valentine (1999), Seasonal patterns and environmental control of carbon dioxide and water vapor exchange in an ecotonal boreal forest, *Global Change Biol.*, *5*, 891-902.

Ingersoll, A.P. (1983), The atmosphere, *Sci. Am.*, *249*, 162-174.

Ito, A., and T. Oikawa (2002), A simulation model of the carbon cycle in land ecosystems (Sim-CYCLE): a description based on dry-matter production theory and plot-scale validation, *Ecol. Modell.*, *151*, 143-176.

Jarvis, P.G., and J.W. Leverenz (1983), Production of temperate, deciduous and evergreen forests in O.L. Lange, C.B. Osmond, and H. Ziegler, editors. *Physiological plant ecology IV.* New York: Springer-Verlag, 133-144.

Katul, G., R. Leuning, and R. Oren (2003), Relationship between plant hydraulic and biochemical properties derived from a steady-state coupled water and carbon transport model, *Plant Cell Environ.*, *26*, 339-350.

Keeling, C.D., and T.P. Whorf (2002), Atmospheric CO_2 records from sites in the SIO air sampling network. In *Trends: A Compendium of Data on Global Change*. Carbon Dioxide Information Analysis Center, Oak Ridge National Laboratory, U.S. Department of Energy, Oak Ridge, Tenn., U.S.A.

Kruijt, B., J.A. Elbers, C. von Randow, A.C. Araujo, P.J. Oliveira, A. Culf, A.O. Manzi, A.D. Nobre, P. Kabat, and E.J. Moors (2004), The robustness of eddy correlation fluxes for Amazon rain forest conditions, *Ecol. Appl.*, *14*, S101-S113.

Kucharik, C.J., J.A. Foley, C. Delire, V.A. Fisher, M.T. Coe, J. Lenters, C. Young-Molling, N. Ramankutty, J.M. Norman, and S.T. Gower (2000), Testing the performance of a dynamic global ecosystem model: Water balance, carbon balance and vegetation structure, *Global Biogeochem. Cycles*, *14*, 795-825.

Law, B.E., D.D. Baldocchi, and P.M. Anthoni (1999), Below-canopy and soil CO_2 fluxes in a ponderosa pine forest, *Agric. For. Meteorol.*, *94*, 3-4:171-188.

Le Quere, C., J.C. Orr, P. Monfray, O. Aumont, and G. Madec (2000), Interannual variability of the oceanic sink of CO_2 from 1979 through 1997, *Global Biogeochem. Cycles*, *14*, 1247-1265.

Leuning, R. (1990), Modeling stomatal behavior and photosynthesis of Eucalyptus grandis, *Australian J. Plant Phys.*, *17*, 159-175.

Lucht, W., I.C. Prentice, R.B. Myneni, S. Sitch, P. Friedlingstein, W. Cramer, P. Bousquet, W. Buermann, and B. Smith (2002), Climatic control of the high-latitude vegetation greening trend and the Pinatubo effect, *Science, 296*, 1687-1689.

Markkanen, T., Ü. Rannik, P. Keronen, T. Suni, and T. Vesala (2001), Eddy covariance fluxes over a boreal Scots pine forest, *Boreal Environ. Res., 6*, 65-78.

McGuire, A.D., J.M. Melillo, L.A. Joyce, D.W. Kicklighter, A.L. Grace, B. Moore III, and C.J. Vorosmarty (1992), Interactions between carbon and nitrogen dynamics in estimating net primary production for potential vegetation in North America, *Global Biogeochem. Cycles*, *6*, 101-124.

Mitchell, T.D., T.R. Carter, P.D. Jones, M. Hulme, and M. New (2003), A comprehensive set of high-resolution grids of monthly climate for Europe and the globe: the observed record (1901-2000) and 16 scenarios (2001-2100), *J. Clim.*, submitted.

Monteith, J.L. (1965), Evaporation and the environment. En: The state and movement of water in living organisms. *Proceedings of the 19th Symposium, Society of Experimental Biology.* London: Cambridge Univesity Press.

Montieth, J.L. (1972), Solar radiation and production in tropical ecosystems, *J. Appl. Ecol.*, *9*, 747-766.

Montieth, J.L. (1977), Climate and efficiency of crop production in Britain, *Philosophical Transaction Royal Society of London, Ser. B*, 277-294.

Myneni, R.B., R.R. Nemani, and S.W. Running (1997a), Estimation global leaf area index and absorped PAR using radiative transfer models, *IEEE Trans. Geosci. Remote Sens.*, *35*, 1380-1393.

Myneni, R.B., C.D. Keeling, C.J. Tucker, G. Asrar, and R.R. Nemani (1997b), Increased plant growth in the northern high latitudes from 1981 to 1991, *Nature*, *386*, 698-702.

Neilson, R.P. (1995), A model for predicting continental scale vegetation distribution and water balance, *Ecol. Appl.*, *5*, 362-385.

Nemani, R.R., C.D. Keeling, H. Hasimoto, W.M. Jolly, S.C. Piper, C.J. Tucker, R.B. Myneni, and S.W. Running (2003), Climate-Driven Increases in Global Terrestrial Net Primary Production from 1982 to 1999, *Science*, *300*, 1560-1563.

Parton, W.J., J.M.O. Scurlock, D.S. Ojima, T.G. Gilmanov, R.J. Scholes, D.S. Schimel, T. Kirchner, J.C. Menaut, T. Seastedt, E.G. Moya, A. Kamnalrut, and J.L. Kinyamario (1993), Observations and modeling of biomass and soil organic matter dynamics for the grassland biome worldwide, *Global Biogeochem. Cycles*, *7*, 785-809.

Potter, C.S., J.T. Randerson, C.B. Field, P.A. Matson, P.M. Vitousek, H.A. Mooney, and S.A. Klooster (1993), Terrestrial ecosystem production: A process model based on global satellite and surface data, *Global Biogeochem. Cycles*, *7*, 811-841.

Potter, C.S., S. Klooster, R.B. Myneni, V. Genovese, P.N. Tan, and V. Kumar (2003), Continental scale comparisons of terrestrial carbon sinks estimated from satellite data and ecosystem modeling 1982–1998, *Global Planetary Change*, *39*, 201–213.

Prince, S.D. (1991), A model of regional primary production for use with coarse resolution satellite data, *Int. J. Remote Sens.*, *12*, 1313-1330.

Prince, S.D., and S.M. Goward (1995), Global primary production: A remote sensing approach, *J. Biogeogr.*, *22*, 815-835.

Raich, J., E. Rastetter, J. Melillo, B.J. Peterson, D. Kicklighter, P.A. Steudler, B. Moore, C. Vörösmarty, and A. Grace (1991), Potential net primary production in south America: Application of a global model, *Ecol. Appl.*, *4*, 399-429.

Rampino, M.R., and S. Self (1984), The atmospheric effects of El Chichón, *Sci. Am.*, *250*, 48-57

Ruimy, A., B. Saugier, and G. Dedier (1994), Methodology for the estimation of terrestrial net primary production from remotely sensed data, *J. Geophys. Res.*, *99*, 5263-5283.

Ruimy, A., G. Dedieu, and B. Saugier (1996), TURC: a diagnostic model of continental gross primary production and net primary production, *Global Biogeochem. Cycles*, *10*, 269-286.

Ruimy, A., L. Kergoat, A. Bondeau, and the participants of the Potsdam NPP Model Intercomparison (1999), Comparing global models of terrestrial net primary production (NPP): analysis of differences in light absorption and light-use efficiency, *Global Change Biol.*, *5*, 56-64.

Running, S.W., R.R. Nemani, J.M. Glassy, and P.E. Thornton (1999), MODIS Daily Photosynthesis (PSN) and Annual Net Primary Production (NPP) Product (Mod17): *Algorithm Theoretical Basis Document. V. 4.0*.

Runyon, J., R.H. Waring, S.N. Goward, and J.M. Welles (1994), Environmental limits on net primary production and light-use efficiency across the Oregon transect, *Ecol. Appl.*, *4*, 226-237.

Saxton, K.E., W.J. Rawls, J.S. Romberger, and R.I. Papendick (1986), Estimating generalized soil-water characteristics from texture, *Soil Sci. Soc. Am.*, *50*, 1031-1036.

Self, S., J.X. Zhao, R.E. Holasek, R.C. Torres, and A.J. King (1996), The atmospheric impact of the 1991 Mount Pinatubo eruption, in Newhall, C.G., and R.S. Punongbayan (eds.), 1996, *Fire and mud: Eruptions and lahars of Mt. Pinatubo, Philippines*. Philippine Institute of Volcanology and Seismology, Quezon City and University of Washington Press, Seattle, 1126.

Sellers, P.J., J.A. Berry, G.J. Collatz, C.B. Field, and F.G. Hall (1992), Canopy reflectance, Photosynthesis and transpiration. III. Area analysis using improved leaf models and a new canopy integration scheme, *Remote Sens. Environ.*, *42*, 187-216.

Sellers, P.J., D.R. Randall, G.J. Collatz, J.A. Berry, C.B. Field, D.A. Dazlich, and G.D. Collelo (1996), A revised land-surface parameterization (SiB2) for GCMs. Part 1: Model formulation, *J. Clim.*, *9*, 676-705.

Sitch, S., B. Smith, I.C. Prentice, A. Arneth, A. Bondeau, W. Cramer, J.O. Kaplan, S. Levis, W. Lucht, M.T. Sykes, K. Thonicke, and S. Venevsky (2003), Evaluation of ecosystem dynamics, plant geography and terrestrial carbon cycling in the LPJ dynamic global vegetation model, *Global Change Biol.*, *9*, 161-185.

Suyker, A.E., and S.B. Verma (2001), Year-round observations of the net ecosystem exchange of carbon dioxide in a native tallgrass prairie, *Global Change Biol.*, *7*, 279-289.

Valentini, R., G. Matteucci, A.J. Dolman, E.D. Schulze, C. Rebmann, E.J. Moors, A. Granier, P. Gross, N.O. Jensen, K. Pilegaard, A. Lindroth, A. Grelle, C. Bernhofer, T. Grunwald, M. Aubinet, R. Ceulemans, A.S. Kowalski, T. Vesala, U. Rannik, P. Berbigier, D. Loustau, J. Gudmundsson, H. Thorgeirsson, A. Ibrom, K. Morgenstern, R. Clement, J. Moncrieff, L. Montagnani, S. Minerbi, and P.G. Jarvis (2000), Respiration as the main determinant of carbon balance in European forests, *Nature, 404*, 861-865.

Warnant, P., L. François, D. Strivay, and J.C. Gérard. (1994), CARAIB: a global model of terrestrial biological production, *Global Biogeochem. Cycles*, *8*, 255-270.

Webb, R.S., C.E. Rosenzweig, and E.R. Levine (1993), Specifying land surface characteristics in general circulation models: soil profile data set and derived water-holding capacities, *Global Biogeochem. Cycles*, *7*, 97-108.

Wilson, K.B., and D.D. Baldocchi (2001), Comparing independent estimates of carbon dioxide exchange over 5 years at a deciduous forest in the southeastern United States, *J. Geophs. Res.*, *106*, 34167-34178.

Wofsy, S.C., M.L. Goulden, J.W. Munger, S.M. Fan, P.S. Bakwin, B.C. Daube, S.L. Bassow, and F.A. Bazzaz (1993) Net exchange of CO_2 in a midlatitude forest, *Science*. *260*, 5112, 1314-1317.

Wullschleger, S.D. (1993), Biochemical limitations to carbon assimilation in C_3 plants – A retrospective analysis of the A/C_i curves from 109 species, *J. Exper. Botany*, *44*, 907-920.

Zheng, D.L., S.D. Prince, and R. Wright (2003), Terrestrial net primary production estimates for 0.5 degree grid cells from field observations – a contribution to global biogeochemical modeling, *Global Change Biol.*, *9*, 46-64.

Zobler, L. (1986), *A World Soil File for Global Climate Modeling*. NASA Technical Memorandum 87802. New York: NASA Goddard Institute for Space Studies.

Zhou, L., C.J. Tucker, R.K. Kaufmann, D. Slayback, N.V. Shabanov, and R.B. Myneni (2001), Variations in northern vegetation activity inferred from satellite data of vegetation index during 1981 to 1999, *J. Geophys. Res.*, *106*, 20069-20083.

Table 1-1 Definitions of parameters used in the Stress calculation

Parameter	Definition	Unit
P	Photosynthesis rate	$\mu mol/m^2/s$
Ps	Ribulose-biophosphate carboxylase oxygenase limited rate	$\mu mol/m^2/s$
Pl	Light-limited rate of photosynthesis	$\mu mol/m^2/s$
Pm	Capacity for export or utilization of photosynthetic products	$\mu mol/m^2/s$
Rd	Dark respiration	$\mu mol/m^2/s$
Vcmax	Maximum rate of carboxylation	$\mu mol/m^2/s$
$Vcmax_{25}$	Maximum rate of carboxylation at 25°C	$\mu mol/m^2/s$
$Q_{10Vcmax}$	Q10 value of Vcmax (= 2.4)	
Fsoil1	Stress value for Vcmax (range; 0.0-1.0)	
Ψwp	Water potential at the wilting point	m
Ψ	Matric water potential	m
Ψs	Matric water potential at saturation	m
V	Volumetric soil moisture	
B	Slope of the retention curve on a logarithmic graph	
pi	Intercellular CO_2 pressure	Pa
Γ^*	CO_2 compensation point in the absence of dark respiration	Pa
Kc	Michaelis-Menten constants for CO_2	Pa
Kc_{25}	Michaelis-Menten constants for O_2 at 25°C	Pa
Q_{10Kc}	Q10 value of Kc (= 2.1)	
Ko	Michaelis-Menten constants for CO_2	Pa
Ko_{25}	Michaelis-Menten constants for O_2 at 25°C	Pa
Q_{10Ko}	Q10 value of Ko (= 1.2)	
J	A rate of electron transport	$\mu mol\text{-}p\ /m^2/s$
τ	CO_2/O_2 specificity ratio	

Table 1-1 (continued)

Parameter	Definition	Unit
τ_{25}	Atmospheric CO_2/O_2 ratio at 25°C	(Pa/Pa)
$Q_{10\tau}$	Q10 value of τ (= 0.57)	
Oxy	O_2 concentration	(Pa/Pa)
θ_j	Curvature of leaf response of electron transport to irradiance (= 0.7)	
Jmax	Potential rate of electron transport	µmol-p /m^2/s
I_j	PAR effectively absorbed by PSII	µmol-p /m^2/s
g	Total conductance to CO_2	µmol/m^2/s
Gst	Stomatal conductance	µmol/m^2/s
Gbl	Boundary layer conductance	µmol/m^2/s
b, m	Constant values (0.01 and 9.2, respectively)	
Γ	Compensation point	Pa
Fsoil2	Soil water stress for stomatal conductance	
hs	relative air humidity	
Ψfc	Water potential at field capacity	m
P_atm	Atmospheric pressure	Pa
patm	Atmospheric CO_2 pressure	Pa

Table 1-2 Definitions of parameters used in the carbon cycle submodel

Parameter	Definition	Unit
GPP	Gross Primary Production	$gC/m^2/mon$
PAR	Photosynthetically Active Radiation	$MJ/m^2/month$
APAR	Absorbed PAR	$MJ/m^2/month$
FPAR	A Fraction of PAR	
LUEmax	Maximum Light Use Efficiency (0.0-1.0)	gC/MJ
Ra	Autotrophic Respiration	$gC/m^2/mon$
kr	Specific respiration rate (leave, stem, and root)	/month
Cbio	Carbon content of biomass	gC/m^2
fr_g	A fraction of growth respiration in the potential NPP (=0.25)	
LF	Litter fall	$gC/m^2/mon$
kl	Specific litter fall rate (stem, and root)	/month
SD	Soil Decomposition	$gC/m^2/mon$
ki	Maximum decay rate constant of each soil carbon pool	/month
Lc	Effect of lignin content of structural material on structural decomposition	
Cs_i	Carbon content of litter or SOM pool	gC/m^2
D_{tw}	Combined effect of soil water content and temperature on decomposition scalars (0.0-1.0)	
M	Carbon assimilation efficiency of soil microbes	
Tm	Effect of silt plus clay content on active SOM turnover	

Table 1-3 Definitions of parameters used in the hydrology submodel

Parameter	Definition	Unit
W_1	Soil water content of upper layer	mm
W_2	Soil water content of lower layer	mm
β_1, β_2	Partitioning parameters of transpired water extraction from the upper and lower soil layers	
PPT	Potential precipitation (total water flux to upper soil layer, snowmelt + precipitation)	mm
EET	Estimated evapotranspiration	mm
PET	Potential evaportranspiration	mm
RDR	Relative dry rate scalar	
Perc	Percolation from upper to lower soil layer	mm

Table 2 Input data sets used in BEAMS

Parameter	Temporal resolution[a]	Spatial resolution[b]	Details
Temp, Prec, VP	m	0.5 * 0.5 deg	CRU TS 2.0 data-set
SOL, NSW, NLW, WND	d	2.5 * 2.5 deg	NCEP/NCAR reanalysis
fAPAR, LAI	m	0.5 * 0.5 deg	FPAR/LAI derived from GIMMS NDVI data set [c]
Land cover map	c	1.0 * 1.0 deg	NDVI-derived land cover classification [d]
Soil texture, depth	c	1.0 * 1.0 deg	FAO soil texture groups
Elevation	c	10 * 10 min	U. S. Navy (FNOC) 10-minute elevation

[a] m: monthly, d: daily, c: constant; [b] deg: degree, min: minute;

[c] Global Inventory Monitoring and Modeling Studies NDVI data set (Myneni et al., 1997; Zhou et al., 2001; Nemani et al. 2003)

[d] One degree land cover map derived from AVHRR data (DeFries and Townshend,1994)

Table 3 List of GPP comparison sites

Flux site	Latitude	Longitude	Period	Project	Data Providers	Biome Type*
Aberfeldy[1]	56° 36' N	3° 47' W	1997-98	EUROFLUX	R. Clement, J. Moncrieff	Cropland
Brasschaat[1]	51° 18' N	4° 31' E	1998	EUROFLUX	A. Kowalski, N. Shurpali, R. Ceulemans	Cropland
Duke Forest[2]	35° 58' N	79° 5' W	1998	AmeriFlux	C.T. Lai, G. Katul, R. Oren	Mixed Forest
Harvard Forest[3]	42° 32' N	72° 10' W	1992-99	AmeriFlux	J. William, Munger, S. Wofsy	DBF
Hesse Forest[1]	48° 40' N	7° 03' E	1997-99	EUROFLUX	A. Granier	Cropland
Howland Forest[4]	45° 20' N	68° 74' W	1996-97	AmeriFlux	D. Hollinger	Mixed Forest
Hyytiala[1, 5]	61° 50' N	24° 17' E	1997-98	EUROFLUX	T. Markkanen	ENF
Loobos[1]	52° 10' N	5° 44' E	1997-98	EUROFLUX	E. Moors, H. Dolman	Mixed Forest
Manaus[6]	2° 35' S	60° 6' W	1996	EUSTACH	J. Elbers, B. Kruijt, A. Nobre	EBF
Metolius[7]	44° 29' N	121° 37' W	1996-97	AmeriFlux	P. Anthony, B.E. Law	ENF
BOREAS NSA Old Black Spruce[8]	55° 52' N	98° 28' W	1995-98	AmeriFlux	M. Goulden, S. Wofsy	ENF
Norunda[1]	60° 05' N	16° 13' E	1996-97	EUROFLUX	A. Grelle, A. Lindroth	ENF
Shidler[9]	36° 56' N	96° 41' W	1997	AmeriFlux	S. Verma	Grassland
Soroe[1]	55° 29' N	11° 38' E	1997-99	EUROFLUX	Kim Pilegaard, Niels-Otto Jensen	Cropland
Tharandt[1]	50° 57' N	13° 34' E	1997-99	EUROFLUX	T. Grunwald, C. Bernhofer	ENF
Walker Branch[10]	35° 57' N	84° 17' W	1995-98	AmeriFlux	D. Baldocchi, K. Wilson	DBF

Flux site name	Latitude	Longitude	Period	Project	Data Providers	Biome Type*
Aberfeldy[1]	56° 36' N	3° 47' W	1997-98	EUROFLUX	R. Clement, J. Moncrieff	Cropland
Brasschaat[1]	51° 18' N	4° 31' E	1998	EUROFLUX	A. Kowalski, N. Shurpali, R. Ceulemans	Cropland
Duke Forest[2]	35° 58' N	79° 5' W	1998	AmeriFlux	C.T. Lai, G. Katul, R. Oren	Mixed Forest
Harvard Forest[3]	42° 32' N	72° 10' W	1992-99	AmeriFlux	J. William, Munger, S. Wofsy	DBF
Hesse Forest[1]	48° 40' N	7° 03' E	1997-99	EUROFLUX	A. Granier	Cropland
Howland Forest[4]	45° 20' N	68° 74' W	1996-97	AmeriFlux	D. Hollinger	Mixed Forest
Hyytiala[1, 5]	61° 50' N	24° 17' E	1997-98	EUROFLUX	T. Markkanen	ENF
Loobos[1]	52° 10' N	5° 44' E	1997-98	EUROFLUX	E. Moors, H. Dolman	Mixed Forest
Manaus[6]	2° 35' S	60° 6' W	1996	EUSTACH	J. Elbers, B. Kruijt, A. Nobre	EBF
Metolius[7]	44° 29' N	121° 37' W	1996-97	AmeriFlux	P. Anthony, B.E. Law	ENF
BOREAS NSA Old Black Spruce[8]	55° 52' N	98° 28' W	1995-98	AmeriFlux	M. Goulden, S. Wofsy	ENF
Norunda[1]	60° 05' N	16° 13' E	1996-97	EUROFLUX	A. Grelle, A. Lindroth	ENF
Shidler[9]	36° 56' N	96° 41' W	1997	AmeriFlux	S. Verma	Grassland
Soroe[1]	55° 29' N	11° 38' E	1997-99	EUROFLUX	Kim Pilegaard, Niels-Otto Jensen	Cropland
Tharandt[1]	50° 57' N	13° 34' E	1997-99	EUROFLUX	T. Grunwald, C. Bernhofer	ENF
Walker Branch[10]	35° 57' N	84° 17' W	1995-98	AmeriFlux	D. Baldocchi, K. Wilson	DBF

[1]Valentini et al. (2000); [2]Katul et al. (2003); [3]Wofsy et al. (1993); [4]Falge et al. (2002); [5]Markkanen et al. (2001); [6]Kruijt et al. (2004); [7]Law et al. (1999); [8]Backwin et al. (2004); [9]Suyker and Verma (2001);[10]Wilson and Baldocchi (2001)
*DBF is Deciduous Broadleaf Forest; ENF is Evergreen Needleleaf Forest; EBF is Evergreen Broadleaf Forest.

Figure Captions;

Figure 1. Procedure of calculating GPP via the Stress approach outlined in this study.

Figure 2. Schematic diagram of the workings of BEAMS

Figure 3. Seasonal variations in estimated (BEAMS and MOD17) and measured GPP at the Harvard forest site from 1992 to 1999.

Figure 4. Annual BEAMS and MOD17 GPP estimates compared with measurements from 19 flux sites.

Figure 5. Global Stress distributions as estimated by BEAMS, CASA, and MOD17.

Water and temperature (Stress), temperature (Stress_t), and water (Stress_w) stresses are provided in the upper, middle, and lower rows, respectively. All stress results are averaged for the period 1982 to 2000. A high Stress value indicates that plants are under suitable temperature and wetness conditions, while a low value indicates inappropriately low or high temperatures, and/or dry conditions. The grey areas represent regions of desert, ice, or areas of no data.

Figure 6. Spatial variation in annual NPP averaged for the period 1982 to 2000.

The white areas indicate desert, ice cover or areas of no data, while the grey areas are ocean.

Figure 7. Comparison of simulated NPP and measured NPP from the GPPDI database.

The data set includes 9 PFTs, which are grouped according to Land Cover Map of Defries and Townshend [1994].

Figure 8. Global variation in the rate of average annual change in NPP for the period 1982 to 2000.

The white areas indicate desert, ice cover or areas of no data, while grey areas are ocean.

Figure 9. Results of the sensitivity analysis for the influence of various input data on NPP trends.

The white areas indicate desert, ice cover or areas of no data, while grey areas are ocean.

Figure 10. Global variation in the rate of annual change of 8 different time-series inputs.

The white areas indicate desert, ice cover or areas of no data, while grey areas are ocean.

Figure 11. Temporal variation in NEP anomaly estimated by BEAMS, and terrestrial carbon flux anomaly estimated by the top-down approach of Bousquet et al. [2000] for the period 1983 to 1997.

Figure 12. Results of sensitivity analysis for inter-annual NEP variations for (a) satellite and climate data, and (b) five different climate parameters.

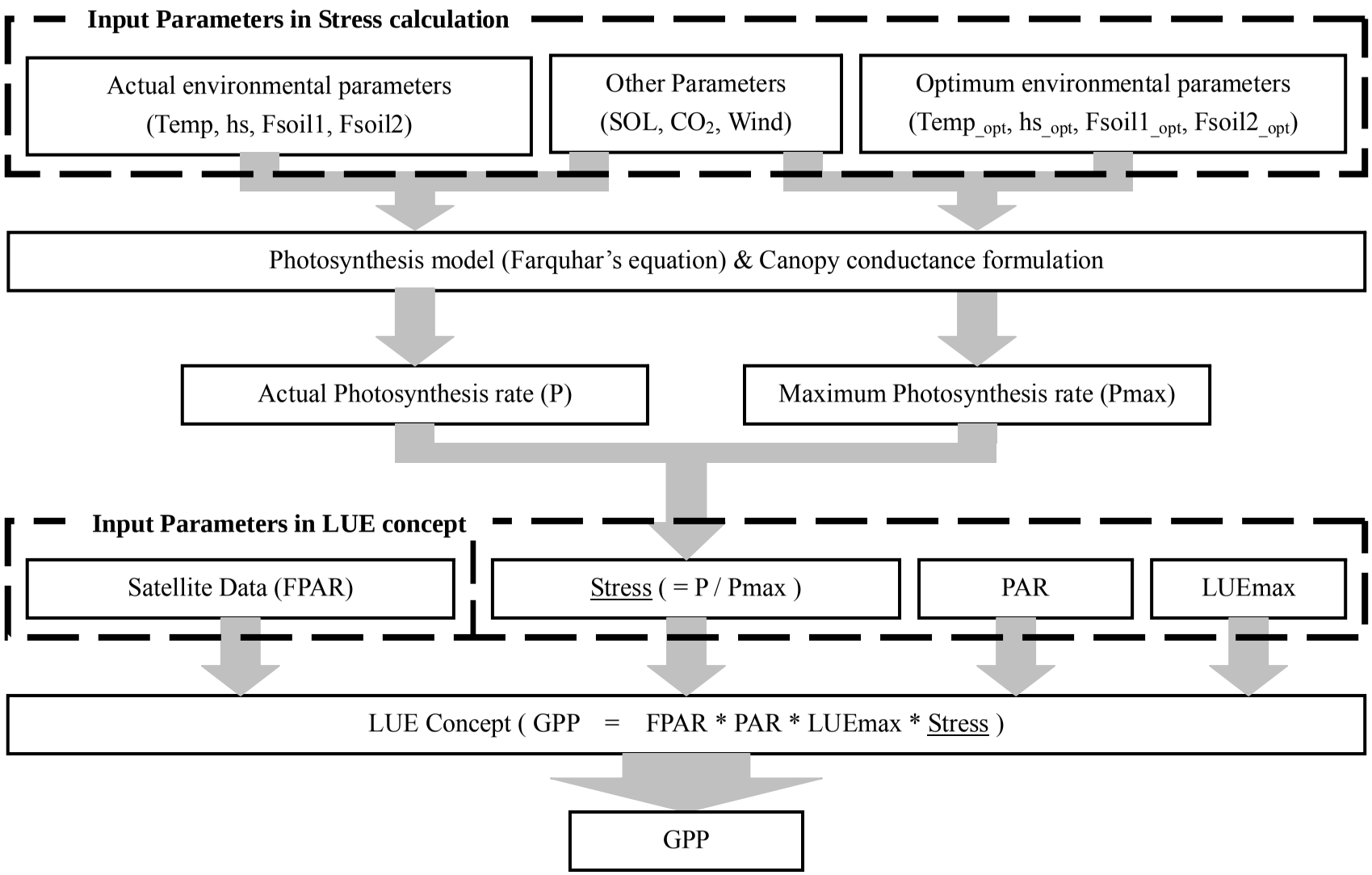

Figure 1. Procedure of calculating GPP via the Stress approach outlined in this study.

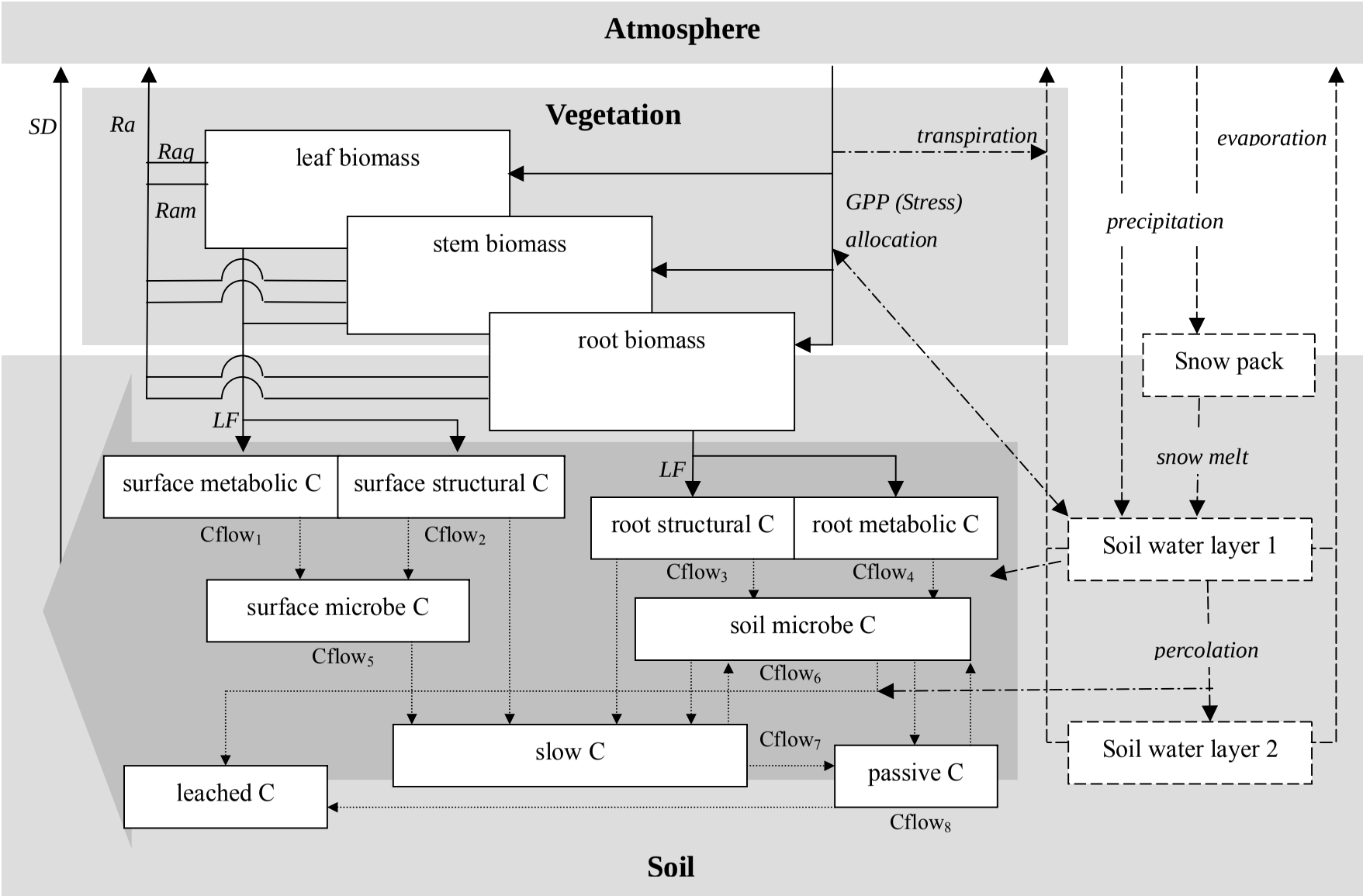

Figure 2. Schematic diagram of the workings of BEAMS

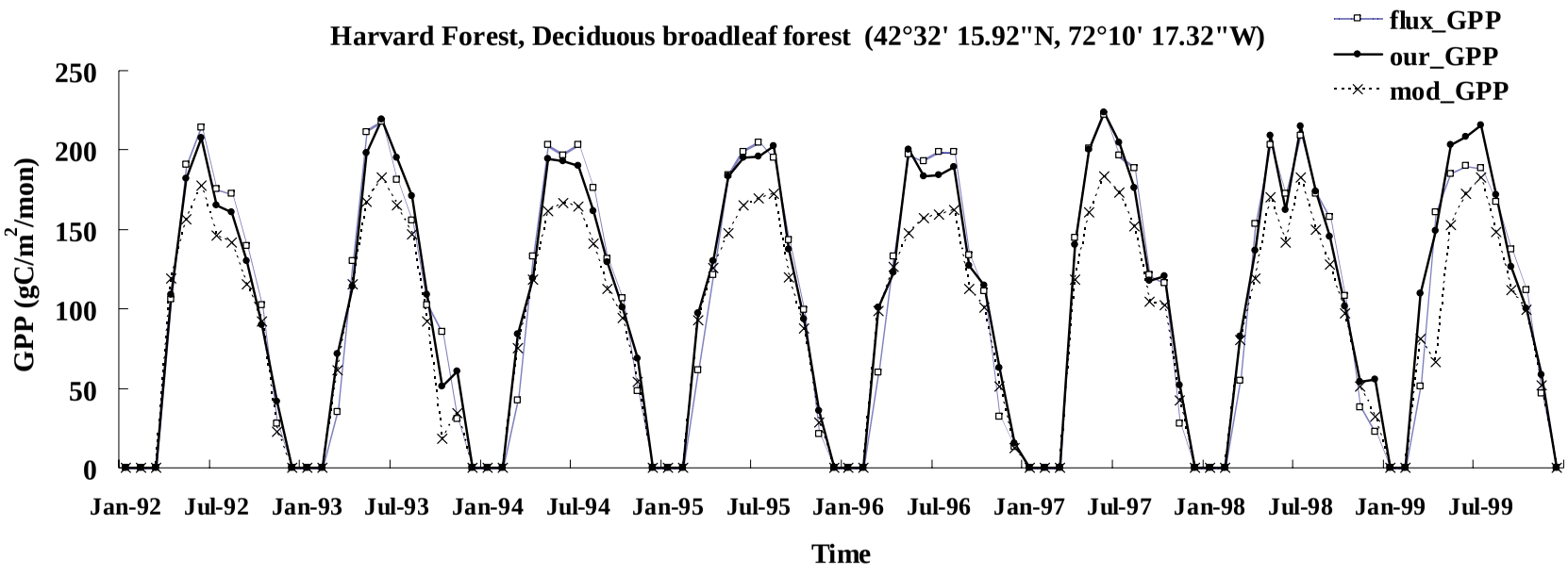

Figure 3. Seasonal variations in estimated (BEAMS and MOD17) and measured GPP at the Harvard forest site from 1992 to 1999.

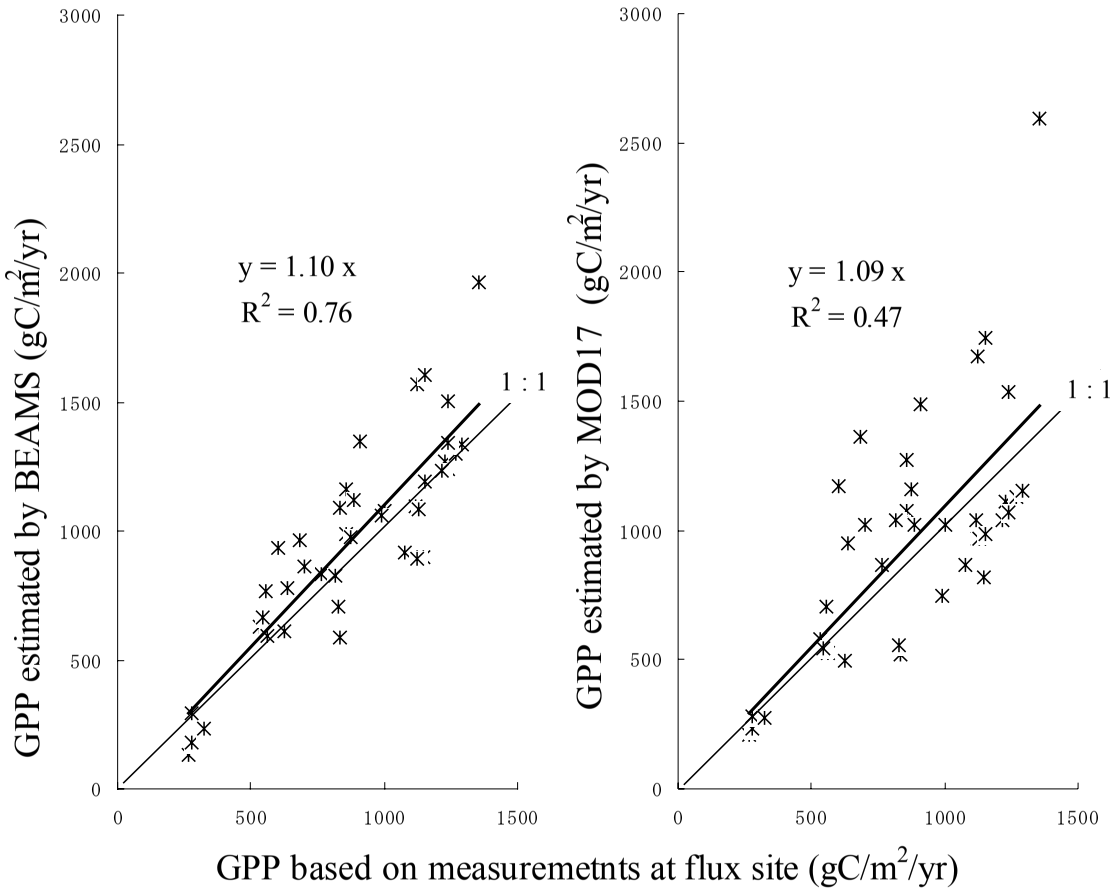

Figure 4. Annual BEAMS and MOD17 GPP estimates compared with measurements from 19 flux sites.

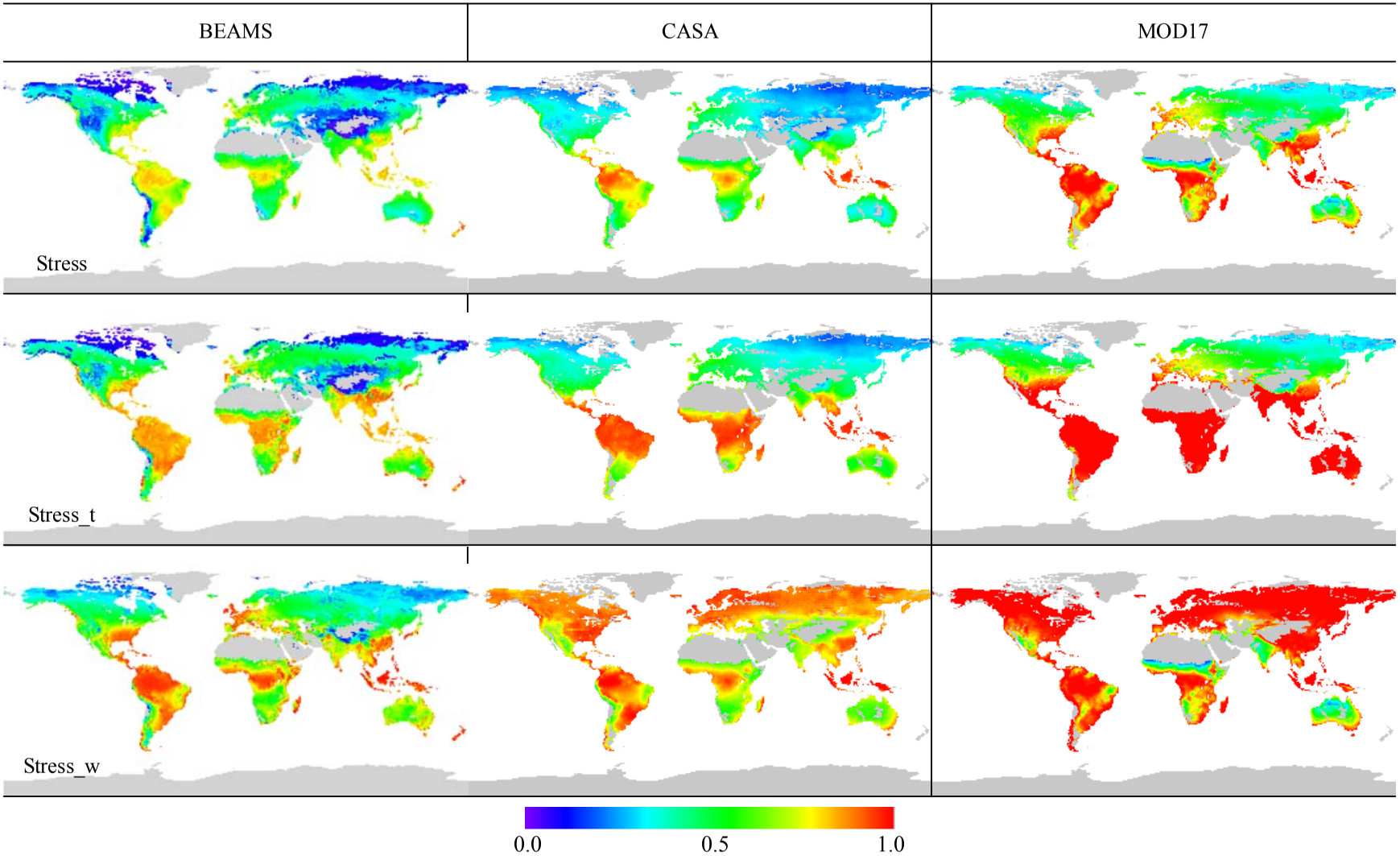

Figure 5. Global Stress distributions as estimated by BEAMS, CASA, and MOD17.

Water and temperature (Stress), temperature (Stress_t), and water (Stress_w) stresses are provided in the upper, middle, and lower rows, respectively. All stress results are averaged for the period 1982 to 2000. A high Stress value indicates that plants are under suitable temperature and wetness conditions, while a low value indicates inappropriately low or high temperatures, and/or dry conditions. The grey zones represent regions of desert, ice, or areas of no data.

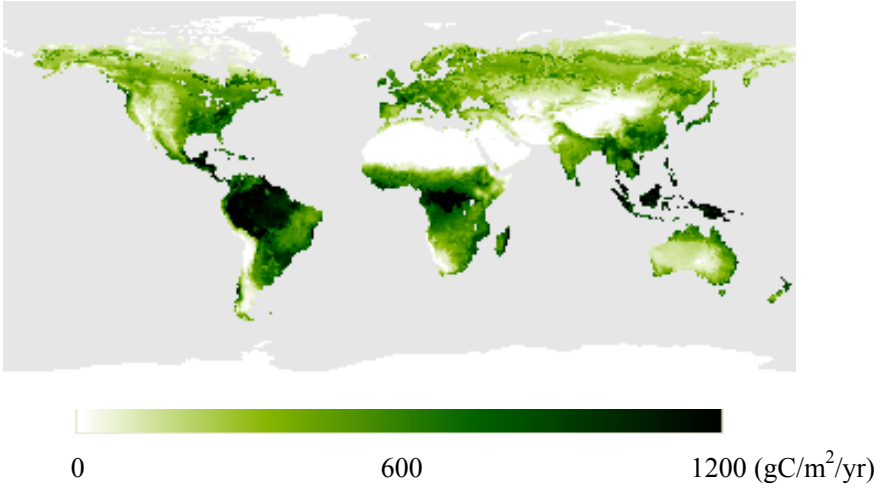

Figure 6. Spatial variation in annual NPP averaged for the period 1982 to 2000.

The white areas indicate desert, ice cover or areas of no data, while the grey areas are ocean.

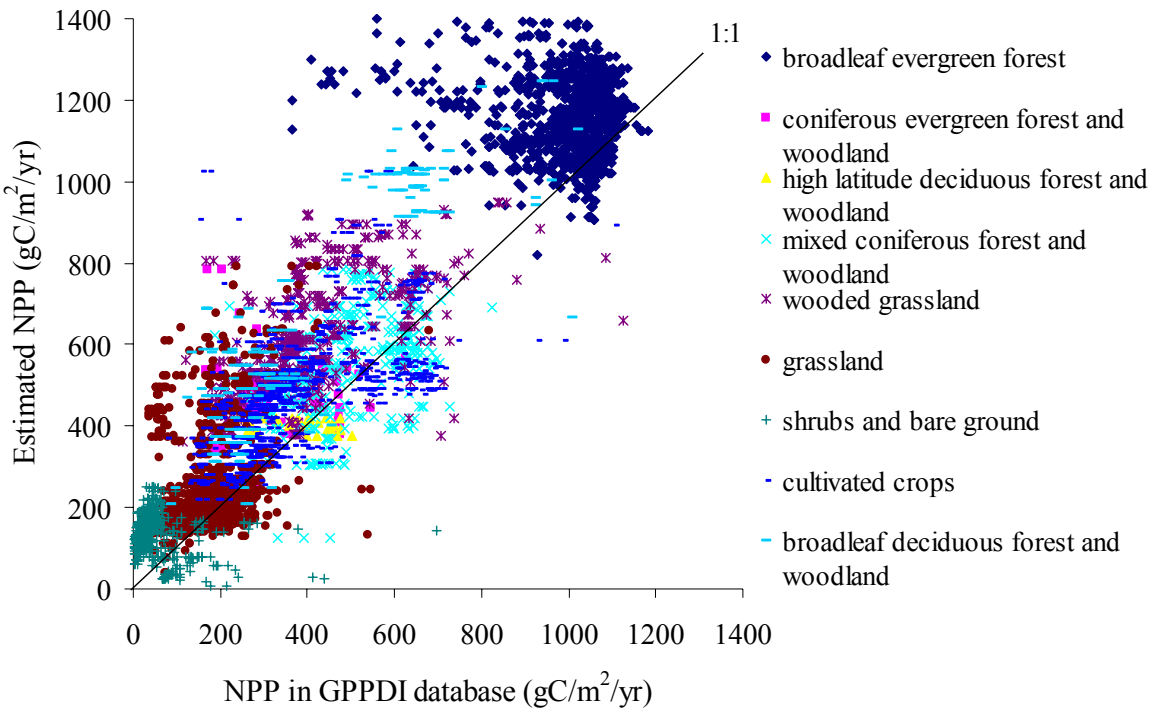

Figure 7. Comparison of simulated NPP and measured NPP from the GPPDI database.

The data set includes 9 PFTs, which are grouped according to Land Cover Map of Defries and Townshend [1994].

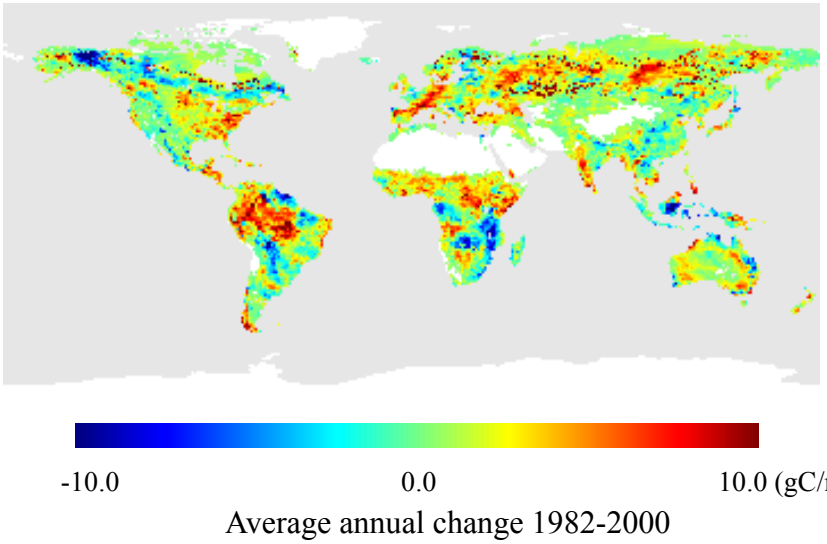

Figure 8. Global variation in the rate of average annual change in NPP for the period 1982 to 2000. The white areas indicate desert, ice cover or areas of no data, while grey areas are ocean.

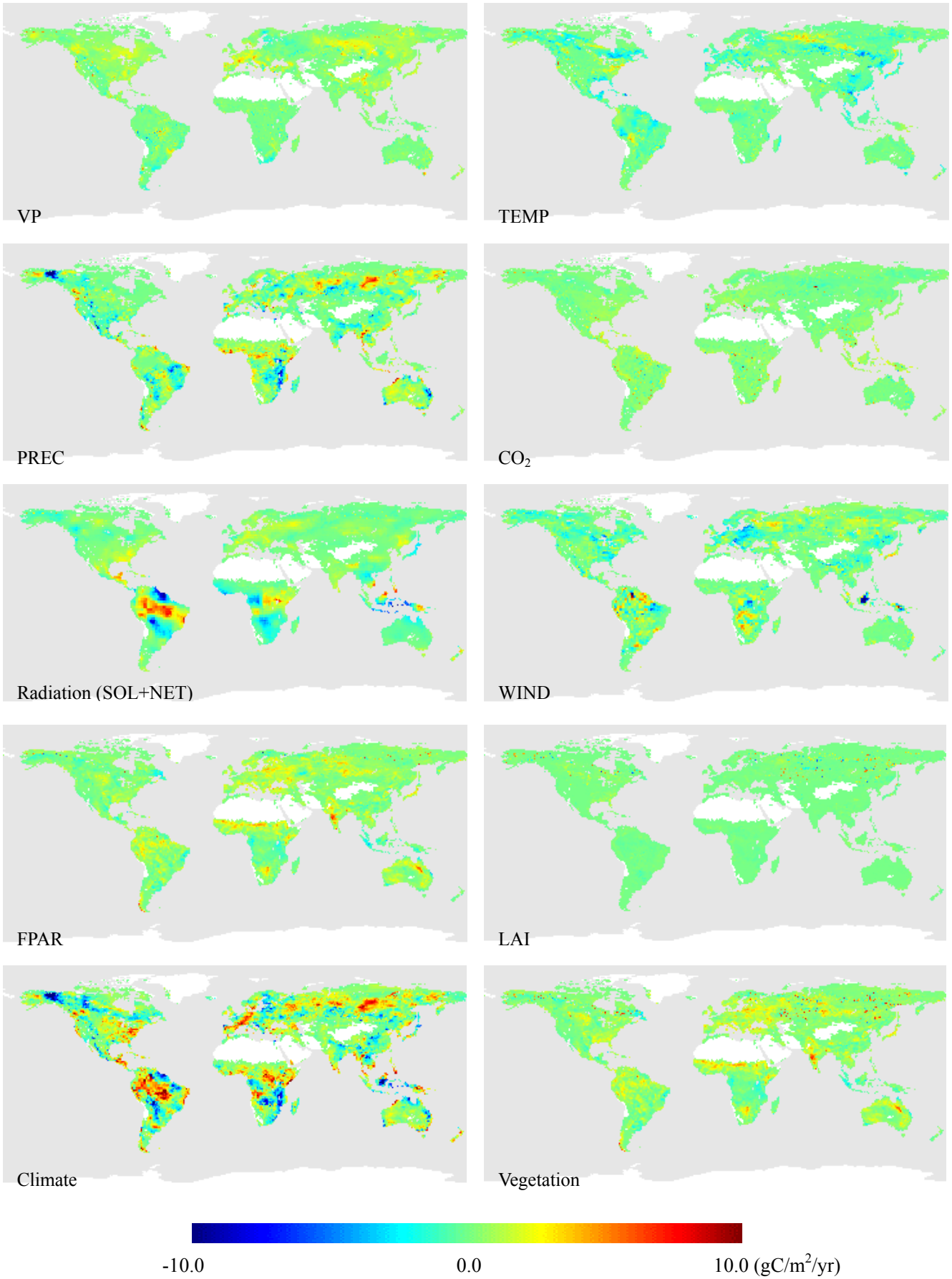

Figure 9. Results of the sensitivity analysis for the influence of various input data on NPP trends. The white zones indicate desert, ice cover or areas of no data, while grey areas are ocean.

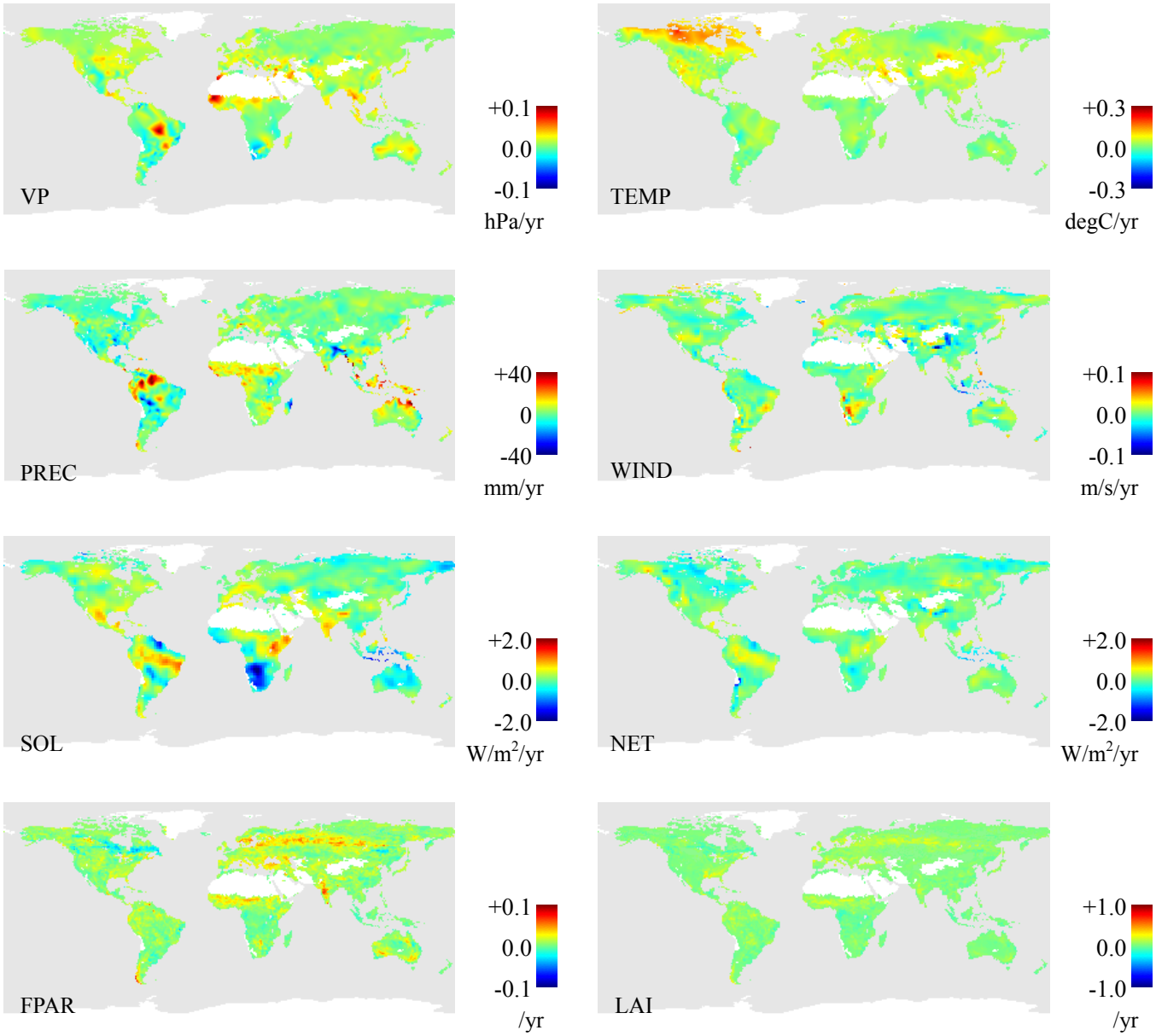

Figure 10. Global variation in the rate of annual change of 8 different time-series inputs. The white areas indicate desert, ice cover or areas of no data, while grey areas are ocean.

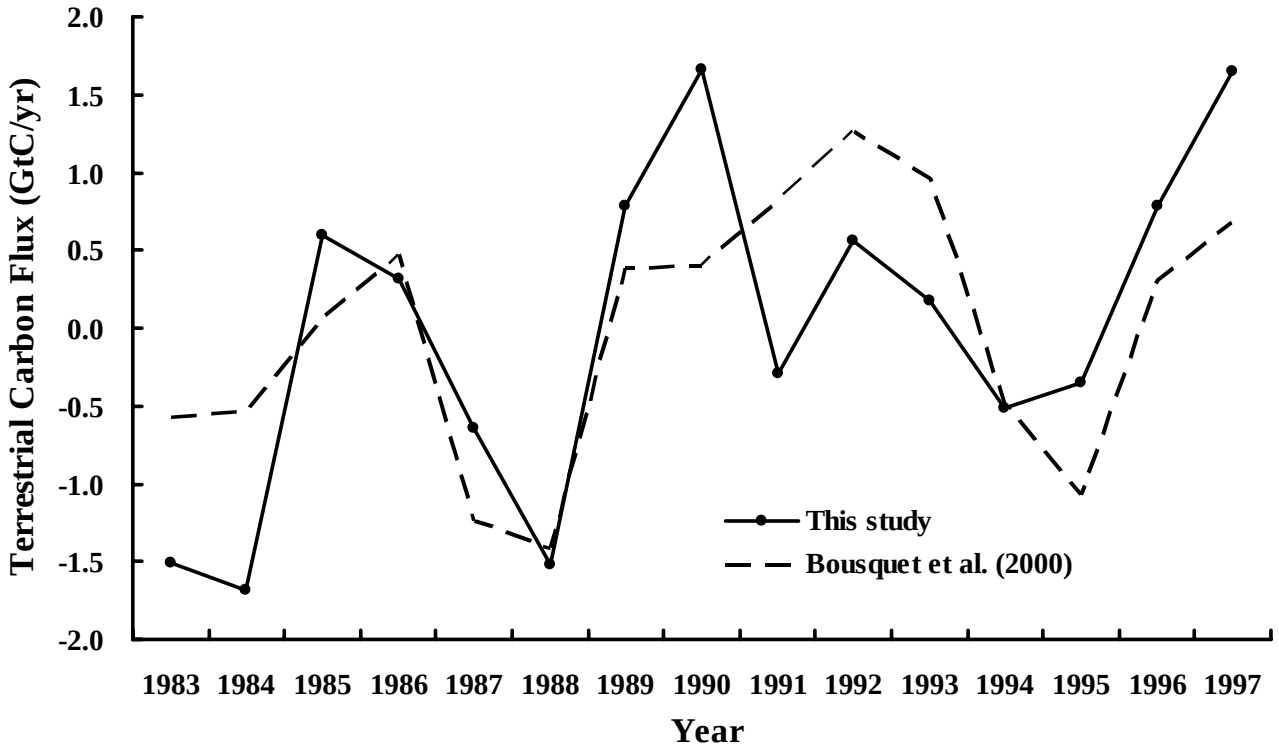

Figure 11. Temporal variation in NEP anomaly estimated by BEAMS and terrestrial carbon flux anomaly estimated by the top-down approach of Bousquet et al. [2000] for the period 1983 to 1997.

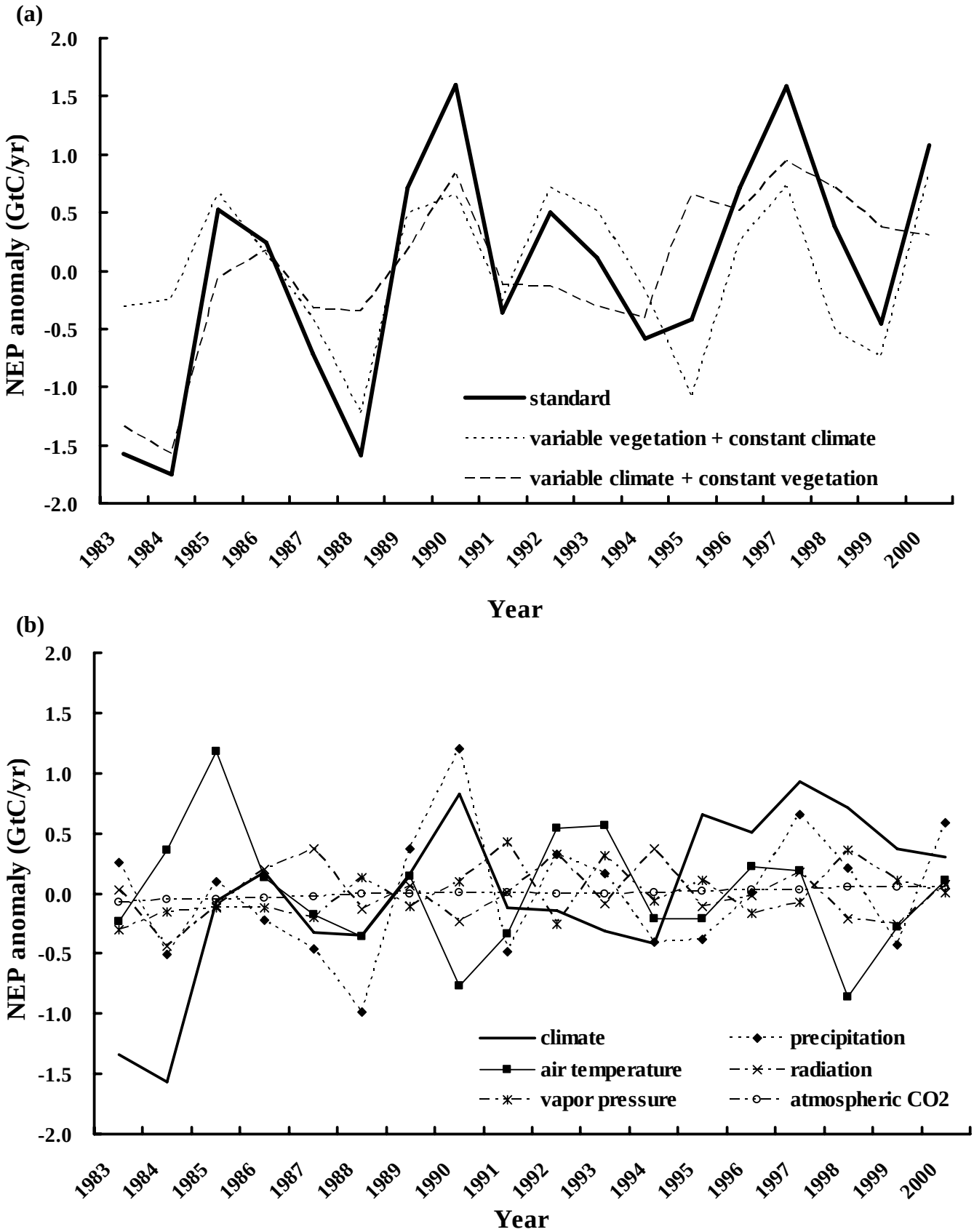

Figure 12. Results of sensitivity analysis for inter-annual NEP variations for (a) vegetation and climate data, and (b) for five different climate parameters.